

# EMBEDDED MINIMAL DISKS

TOBIAS H. COLDING AND WILLIAM P. MINICOZZI II

## CONTENTS

<b>Part I. The main theorem - the limit foliation and the singular curve</b>	1
I.1. Estimates for multi-valued minimal graphs	4
I.2. Towards removability of singularities	8
I.3. Existence of multi-valued graphs and the one-sided curvature estimate	10
I.4. Regularity of the singular set and Theorem I.0.5	14
<b>Part II. The proof of the existence of multi-valued graphs</b>	16
II.1. The proof of existence of small multi-valued graphs - Theorem II.0.14	19
II.2. The estimate between the sheets and the extension of multi-valued graphs	25
<b>Part III. The proof of the one-sided curvature estimate</b>	27
<b>Part IV. The local case - when singular limit laminations can occur</b>	29
References	32

## Part I. The main theorem - the limit foliation and the singular curve

This paper is a survey of our results about embedded minimal disks. Unlike our expository article [CM15], this paper is intended for readers with some background knowledge on minimal surfaces. However, even an expert reader may find it worthwhile to look at [CM15] first.

Let us start with two key examples of embedded minimal disks in  $\mathbf{R}^3$ . The first are minimal graphs over simply connected domains and the second is the double spiral staircase (cf. [CM15]) known as the helicoid.

**Example 1:** Graphs of functions  $u : \Omega \rightarrow \mathbf{R}$  where  $\Omega \subset \mathbf{R}^2$  is simply connected and  $u$  satisfies the second order nonlinear elliptic equation in divergence form (the so-called minimal surface equation)

$$\operatorname{div} \left( \frac{\nabla u}{\sqrt{1 + |\nabla u|^2}} \right) = 0. \quad (\text{I.0.1})$$

**Example 2:** (Helicoid). See fig. 1. The minimal surface in  $\mathbf{R}^3$  parametrized by

$$(s \cos t, s \sin t, -t) \text{ where } s, t \in \mathbf{R}. \quad (\text{I.0.2})$$

---

The first author was partially supported by NSF Grant DMS 9803253 and an Alfred P. Sloan Research Fellowship and the second author by NSF Grant DMS 9803144 and an Alfred P. Sloan Research Fellowship.

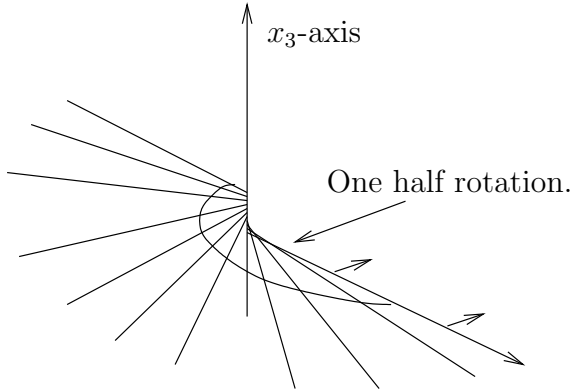


FIGURE 1. The helicoid is obtained by gluing together two  $\infty$ -valued graphs along a line. The two multi-valued graphs are given in polar coordinates by  $u_1(\rho, \theta) = -\theta$  and  $u_2(\rho, \theta) = -\theta + \pi$ . In either case  $w(\rho, \theta) = -2\pi$ .

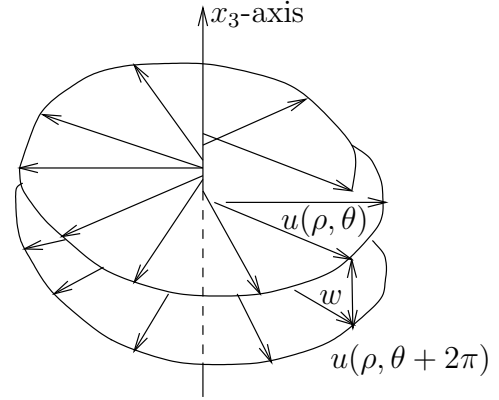


FIGURE 2. The separation of a multi-valued graph. (Here the multi-valued graph is shown with negative separation.)

One of our main theorems is that every embedded minimal disk can either be modelled by a minimal graph or by a piece of the helicoid depending on whether the curvature is small or not; see Theorem I.0.5 below. We will in this survey discuss some of the ingredients in the proof of this and how those ingredients fit together.

To be able to discuss the helicoid some more and in particular give a precise meaning to that it is like a double spiral staircase, we will need the notion of a multi-valued graph; see fig. 2. Let  $D_r$  be the disk in the plane centered at the origin and of radius  $r$  and let  $\mathcal{P}$  be the universal cover of the punctured plane  $\mathbf{C} \setminus \{0\}$  with global polar coordinates  $(\rho, \theta)$  so  $\rho > 0$  and  $\theta \in \mathbf{R}$ . An  $N$ -valued graph of a function  $u$  on the annulus  $D_s \setminus D_r$  is a single valued graph over

$$\{(\rho, \theta) \mid r \leq \rho \leq s, |\theta| \leq N\pi\}. \quad (\text{I.0.3})$$

The multi-valued graphs that we will consider will never close up; in fact they will all be embedded. Note that embedded corresponds to that the separation never vanishes. Here the separation (see fig. 2) is the function given by

$$w(\rho, \theta) = u(\rho, \theta + 2\pi) - u(\rho, \theta). \quad (\text{I.0.4})$$

If  $\Sigma$  is the helicoid, then  $\Sigma \setminus x_3\text{-axis} = \Sigma_1 \cup \Sigma_2$ , where  $\Sigma_1, \Sigma_2$  are  $\infty$ -valued graphs.  $\Sigma_1$  is the graph of the function  $u_1(\rho, \theta) = -\theta$  and  $\Sigma_2$  is the graph of the function  $u_2(\rho, \theta) = -\theta + \pi$ . In either case the separation  $w = -2\pi$ . A multi-valued minimal graph is a multi-valued graph of a function  $u$  satisfying the minimal surface equation (I.0.1).

Here, as in [CM6] and [CM8], we have normalized so our embedded multi-valued graphs have negative separation. This can be achieved after possibly reflecting in a plane.

Let now  $\Sigma_i \subset B_{2R}$  be a sequence of embedded minimal disks with  $\partial\Sigma_i \subset \partial B_{2R}$ . Clearly (after possibly going to a subsequence) either (1) or (2) occur:

- (1)  $\sup_{B_R \cap \Sigma_i} |A|^2 \leq C < \infty$  for some constant  $C$ .  
 (2)  $\sup_{B_R \cap \Sigma_i} |A|^2 \rightarrow \infty$ .

In (1) (by a standard argument) the intrinsic ball  $\mathcal{B}_s(y_i)$  is a graph for all  $y_i \in B_R \cap \Sigma_i$ , where  $s$  depends only on  $C$ . Thus the main case is (2) which is the subject of the next theorem.

Using the notion of multi-valued graphs, this our main theorem, can now be stated:

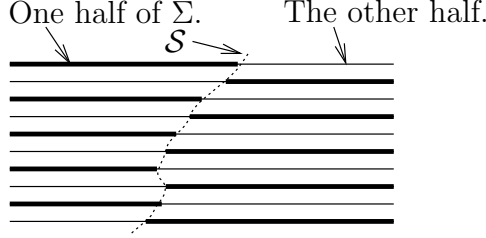


FIGURE 3. Theorem I.0.5 - the singular set,  $\mathcal{S}$ , and the two multi-valued graphs.

**Theorem I.0.5.** (Theorem 0.1 in [CM6]). See fig. 3. Let  $\Sigma_i \subset B_{R_i} = B_{R_i}(0) \subset \mathbf{R}^3$  be a sequence of embedded minimal disks with  $\partial \Sigma_i \subset \partial B_{R_i}$  where  $R_i \rightarrow \infty$ . If  $\sup_{B_1 \cap \Sigma_i} |A|^2 \rightarrow \infty$ , then there exists a subsequence,  $\Sigma_j$ , and a Lipschitz curve  $\mathcal{S} : \mathbf{R} \rightarrow \mathbf{R}^3$  such that after a rotation of  $\mathbf{R}^3$ :

1.  $x_3(\mathcal{S}(t)) = t$ . (That is,  $\mathcal{S}$  is a graph over the  $x_3$ -axis.)
2. Each  $\Sigma_j$  consists of exactly two multi-valued graphs away from  $\mathcal{S}$  (which spiral together).
3. For each  $1 > \alpha > 0$ ,  $\Sigma_j \setminus \mathcal{S}$  converges in the  $C^\alpha$ -topology to the foliation,  $\mathcal{F} = \{x_3 = t\}_t$ , of  $\mathbf{R}^3$ .
4.  $\sup_{B_r(\mathcal{S}(t)) \cap \Sigma_j} |A|^2 \rightarrow \infty$  for all  $r > 0$ ,  $t \in \mathbf{R}$ . (The curvatures blow up along  $\mathcal{S}$ .)

In 2., 3. that  $\Sigma_j \setminus \mathcal{S}$  are multi-valued graphs and converges to  $\mathcal{F}$  means that for each compact subset  $K \subset \mathbf{R}^3 \setminus \mathcal{S}$  and  $j$  sufficiently large  $K \cap \Sigma_j$  consists of multi-valued graphs over (part of)  $\{x_3 = 0\}$  and  $K \cap \Sigma_j \rightarrow K \cap \mathcal{F}$  in the sense of graphs.

Theorem I.0.5 (as many of the other results discussed below) is modelled by the helicoid and its rescalings. Take a sequence  $\Sigma_i = a_i \Sigma$  of rescaled helicoids where  $a_i \rightarrow 0$ . The curvatures of this sequence are blowing up along the vertical axis. The sequence converges (away from the vertical axis) to a foliation by flat parallel planes. The singular set  $\mathcal{S}$  (the axis) then consists of removable singularities.

Of the many different paths that one could choose through our results about embedded minimal disks, we have chosen here one which discusses some of our more elementary results in greater detail and then only gives a very rough overview of some of our key results which are more difficult. Our hope is that by doing so this survey can serve as a reading guide for our papers where the reader is eased into the subject and then is shown the anatomy of the proof of our main theorem.

One of these more elementary themes is that of analysis of multi-valued embedded minimal graphs. From estimates on the growth and decay of the separation between consecutive sheets of such graphs to the results about why such graphs are proper in a certain qualitative sense

if they are contained in larger embedded minimal disks. These results about multi-valued graphs are among what is discussed in some detail in the first part where we also discuss some of the other main results that go into the proof of our main theorem that any embedded minimal disk is either a graph of a function or can be approximated by a piece of a helicoid. In addition, we also discuss in some detail in the first part why the singular set, that is the set of points of large curvature in an embedded minimal disk, must all be contained in a curve which is a Lipschitz graph over a straight line.

In the second part we come to a less elementary result. Namely, that of why near a point of large curvature of an embedded minimal disk there must inside the disk be a small multi-valued graph. Here small means on the scale of one over the square-root of the maximum of the curvature. The much less elementary, but key, result of why such small multi-valued graphs extend to large ones is only discussed very briefly in the second section of that second part.

In the third part we discuss the crucial one-sided curvature estimate. This is the estimate that gives a cone condition for all the points of large curvature. Namely, given a point of large curvature of an embedded minimal disk, then the cone condition is that all the other points of large curvature must lie within a double convex cone of the initial point of large curvature. Iterating this condition gives that the set of all the points of large curvature is the Lipschitz graph over a straight line. The one-sided curvature estimates uses all the results discussed in the first part.

In the final part we discuss what the differences are between the so-called local and global case. The local case is where we have a sequence of embedded minimal disks in a ball of fixed radius in  $\mathbf{R}^3$  - the global case is where the disks are in a sequence of expanding balls with radii tending to infinity. As we will see in the final part, then in the local case we can get limits with singularities. In the global case this does not happen because in fact any limit is always a foliation by flat parallel planes (this is assuming that the curvatures of the sequence are blowing up).

There are a number of important results that go into the proof of our main theorem about embedded minimal disks that are either not discussed here or are barely mentioned. One of these is why given a point of large curvature in an embedded minimal disk there are points of large curvature nearby above and below. This was one of the key results proven in [CM5] but is quite technical and thus has been omitted from this survey.

Let  $x_1, x_2, x_3$  be the standard coordinates on  $\mathbf{R}^3$ . For  $y \in \Sigma \subset \mathbf{R}^3$  and  $s > 0$ , the extrinsic and intrinsic balls are  $B_s(y), \mathcal{B}_s(y)$ .  $K_\Sigma$  the sectional curvature of a smooth compact surface  $\Sigma$  and when  $\Sigma$  is immersed  $A_\Sigma$  will be its second fundamental form (so when  $\Sigma$  is minimal, then  $|A|^2 = -2K_\Sigma$ ). When  $\Sigma$  is oriented,  $\mathbf{n}_\Sigma$  is the unit normal.

Using Theorems I.0.5, I.3.3, W. Meeks and H. Rosenberg proved that the plane and helicoid are the only complete properly embedded simply-connected minimal surfaces in  $\mathbf{R}^3$ , [MeRo].

## I.1. ESTIMATES FOR MULTI-VALUED MINIMAL GRAPHS

We will later see that, just like the helicoid, general embedded minimal disks with large curvature at some interior point can be built out of multi-valued graphs. This will be

particularly useful once we have a good understanding of general embedded multi-valued minimal graphs. In this section, we discuss three basic, but useful, estimates for such graphs:

- A gradient estimate for the separation which implies sublinear growth of  $w$  when there are enough sheets.
- A curvature estimate for 2-valued minimal graphs whose separation grows sublinearly.
- Sharp logarithmic upper and lower bounds for the separation when there is a growing number of sheets.

(See also [CM7] for further discussion of these estimates, their analogs for minimal annuli, and their implications.)

The first of these basic estimates was obtained in [CM3] where we showed (essentially by a gradient estimate) that the separation between the sheets grows sublinearly (in Theorem I.1.6 below we will discuss an improvement of this when the number of sheets grows sufficiently fast). Precisely, in [CM3] we showed that:

**Proposition I.1.1.** (Proposition II.2.12 in [CM3]). Given  $\alpha > 0$ , there exists  $N_\alpha$  so if  $\Sigma$  is an embedded  $N_\alpha$ -valued minimal graph over  $D_{e^{N_\alpha}R} \setminus D_{e^{-N_\alpha}}$  of  $u$  and  $1 \leq \rho \leq R$ , then

$$\rho^{-\alpha} \leq \frac{w(\rho, 0)}{w(1, 0)} \leq \rho^\alpha. \quad (\text{I.1.2})$$

Thus, choosing  $\alpha < 1$ , (I.1.2) gives the sublinear growth of the separation  $w$ . This sublinear growth of the separation is the main benefit of having at least  $N_\alpha$  sheets. It comes from integrating the gradient bound proven in Proposition II.2.12 in [CM3]

$$\frac{|\nabla w|}{|w|} \leq \frac{\alpha}{\rho}. \quad (\text{I.1.3})$$

Many of our results on embedded multi-valued graphs apply as long as (I.1.2) holds and we have at least two sheets.

To get the better logarithmic bounds on the separation, one needs curvature estimates for embedded multi-valued graphs. It follows from Heinz's curvature estimate for minimal graphs (theorem 2.4 in [CM1]) that (away from its boundary) a multi-valued minimal graph has quadratic curvature decay

$$|A|^2 \leq C r^{-2}. \quad (\text{I.1.4})$$

This scale-invariant estimate (I.1.4) does not require embeddedness and can easily be seen to be sharp without any further assumptions on the graph. However, using the embeddedness – and, in particular, the sublinear growth of the separation that embeddedness implies – we showed in corollary 2.3 of [CM8] that the curvature of a multi-valued embedded minimal graph decays faster than quadratically. That is, we showed that

$$|A|^2 \leq C r^{-2-5/6} \quad (\text{I.1.5})$$

for embedded 2-valued minimal graphs whose separation grows sublinearly; cf. (I.1.2). (Note that by [CM3], there exists  $N_\alpha$  so this applies to any  $N_\alpha$ -valued embedded minimal graph.) The important point for the applications in [CM8] is that the faster than linear decay on the Hessian of  $u$  that (I.1.5) implies together with the nonlinear form of (I.0.1) gives that  $|\Delta u|$  decays faster than quadratically; see equation (3.6) in [CM8].

The above faster than quadratic bound (I.1.5) used the nonlinearity of the minimal surface equation much like the nonlinearity is needed for proving the Bernstein theorem. In other situations the nonlinearity seems more to add difficulties than being of any help. In those situations one tries to model the minimal surface equation by the Laplace equation and use that from (I.1.5) if  $u$  is a multi-valued solution of the minimal surface equation, then  $|\Delta u|$  decays faster than quadratically so that  $u$  “become more and more like a harmonic function”. We will now take advantage of this to discuss some analysis of such multi-valued solutions that we will need later. This analysis is from [CM8].

The first such result is the following sharp upper and lower logarithmic bound for the separation of a multi-valued graph:

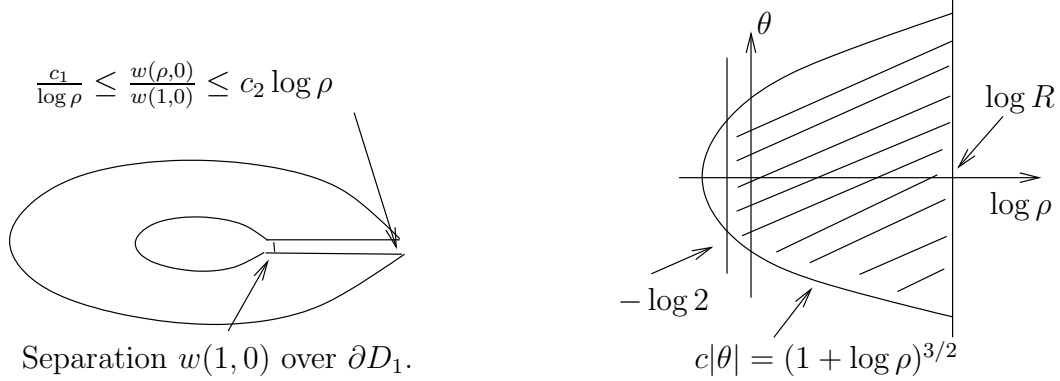


FIGURE 4. Theorem I.1.6: The sharp logarithmic upper and lower bounds for the separation.

FIGURE 5. The domain of  $u$  in Theorem I.1.6 in  $(\log \rho, \theta)$ -coordinates.

**Theorem I.1.6.** (Theorem 1.3 of [CM8]). See fig. 4 and fig. 5. Given  $c > 0$ , there exists  $c_1, c_2$  such that if  $u$  satisfies (I.0.1) on  $\{(\rho, \theta) \mid 1/2 \leq \rho \leq R \text{ and } c|\theta| \leq (1 + \log \rho)^{3/2}\}$  and  $w < 0$  together with a slight condition on the growth of  $u$  and  $w$  (see equation (1.5) in [CM8]), then for  $2 \leq \rho \leq R^{1/2}$

$$\frac{c_1}{\log \rho} \leq \frac{w(\rho, 0)}{w(1, 0)} \leq c_2 \log \rho. \quad (\text{I.1.7})$$

**The idea of the lower bound for the separation**, i.e.,  $w(\rho, 0)/w(1, 0) \geq c_1/\log \rho$ : If  $u$  is as in Theorem I.1.6, then  $w < 0$  is almost harmonic and it can be seen to follow from (I.1.5) and the form of (I.0.1) that so is (the conformally transformed function)  $\tilde{w}(x, y) = w(e^x, y)$ . Moreover,  $\tilde{w} < 0$  is defined on a domain that is conformally close to a half-disk (see lemma 3.2 of [CM8]). Suppose for a moment that  $\tilde{w}$  was actually harmonic and defined on the half-space  $\{x > -\log 2\}$ , then by the mean value equality (see fig. 6) and the sign on  $\tilde{w}$

$$w(e^x, 0) = \tilde{w}(x, 0) = \frac{1}{2\pi x} \int_{\partial D_x(x, 0)} \tilde{w} \leq \frac{1}{2\pi x} \int_{D_1 \cap \partial D_x(x, 0)} \tilde{w}. \quad (\text{I.1.8})$$

By the Harnack inequality, it would then follow from (I.1.8) that  $w(e^x, 0) = \tilde{w}(x, 0) \leq c_1 \tilde{w}(0, 0)/x$ ; which is the desired lower bound. The upper bound follows similarly or by an inversion formula; see section 3 of [CM8].

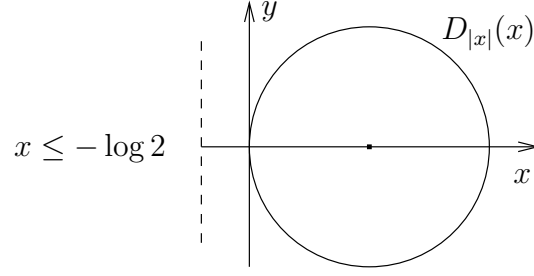


FIGURE 6. Proof of Theorem I.1.6:  
Applying the mean value equality to  
a negative harmonic function defined  
in a half-space.

By Theorem I.1.6, the fastest possible decay for  $w(\rho, 0)/w(1, 0)$  is  $c_1/\log \rho$ . Hence if  $\tilde{w}(x + iy) = w(e^x, y)$ , then the fastest possible decay for  $\tilde{w}(x, 0)/\tilde{w}(0, 0)$  is  $c_1/x$  and as mentioned above, then using (I.1.5) it can be seen that  $\tilde{w}$  is almost harmonic. This decay is achieved for the harmonic function  $\tilde{v}(z) = -\operatorname{Re} z^{-1} = -x/(x^2 + y^2) < 0$  (see fig. 7) and if

$$u(\rho, \theta) = \int_0^\theta v(\rho, y) dy = \int_0^\theta \tilde{v}(\log \rho, y) dy = \int_0^\theta \frac{-\log \rho dy}{(\log \rho)^2 + y^2} = -\arctan \frac{\theta}{\log \rho}, \quad (\text{I.1.9})$$

then the graph of  $u$  is an embedded  $\infty$ -valued harmonic graph lying in a slab, i.e.,  $|u| \leq \pi/2$ , and hence in particular is not proper. Note also that if  $u$  is given by (I.1.9), then  $u_\theta = v$  and  $w/v$  is uniformly bounded above and below. We next want to rule out not only this as an example of one half of an embedded minimal disk, but more generally any  $\infty$ -valued minimal graph in a half-space.

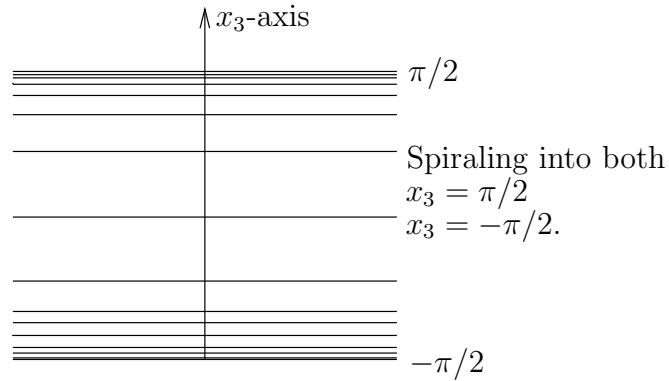


FIGURE 7. Properness; e.g., need  
to rule out that one of the multi-  
valued graphs can contain a graph like  
 $\arctan(\theta/\log \rho)$ , where  $(\rho, \theta)$  are polar  
coordinates.



## I.2. TOWARDS REMOVABILITY OF SINGULARITIES

As mentioned above, we next want to rule out that any  $\infty$ -valued graph which lies in a half-space can be one half of an embedded minimal disk. This is done in Theorem I.2.1 below where the short curves  $\sigma_\theta$  in the minimal disk will connect two multi-valued sub-graphs and thus each sub-graph is essentially one half of the disk. These curves are needed to conclude properness since, as mentioned above, just having one  $\infty$ -valued minimal graph in a slab is not in itself a contradiction.

There is a second key assumption needed to prove this properness: The outer radii  $R_i$  must be going to infinity. We refer to this as the global case. The alternative, the local case, is when the  $R_i$  are bounded. The difference between these two cases is that in the local case it is possible to have non-proper limits which spiral infinitely into a plane. We will return to this in Part IV.

Let us illustrate in an example how these curves  $\sigma$  could be chosen. Here, to be consistent with [CM8], we use the helicoid which spirals downward so  $w < 0$ . If  $\Sigma$  is the helicoid, i.e.,  $\Sigma = (s \cos t, s \sin t, -t)$  where  $s, t \in \mathbf{R}$ , then  $\Sigma \setminus \{s = 0\}$  consists of two  $\infty$ -valued graphs  $\Sigma_1, \Sigma_2$  and the curves  $\sigma_t = \Sigma \cap \{x_3 = t\}$  are short curves connecting the two halves; see fig. 8.

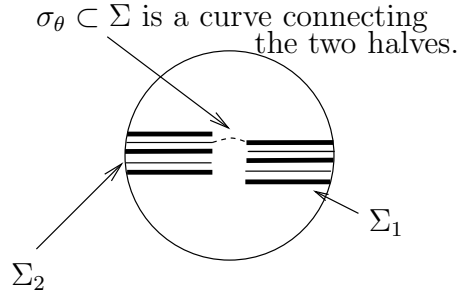


FIGURE 8. The short curves  $\sigma_\theta$  in Theorem I.2.1 connecting the two multi-valued graphs.

**Theorem I.2.1.** (See corollary 1.2 in [CM8] for the precise statement). Let  $\Sigma_i$  be a sequence as in Theorem I.0.5 and suppose that  $\Sigma_{i,1}, \Sigma_{i,2}$  are multi-valued graphs in  $\Sigma_i$  that spiral together (one inside the other). We claim that if  $\Sigma_{i,1}, \Sigma_{i,2}$  can be connected by short curves in  $\Sigma_i$  (see fig. 8), then they cannot spiral into a plane. That is, they cannot accumulate in finite height.

**The idea of the proof of Theorem I.2.1:** Let  $\Sigma_1, \Sigma_2$  be two  $\infty$ -valued graphs of  $u_1, u_2$  that spiral together, are part of an embedded minimal disk, and can be connected by short curves in the disk. We claim that the two graphs must grow out of any half-space. Suppose that they are contained in the half-space  $u_i \geq 0$  and that they spiral downward, i.e.,  $w_i < 0$ ; we will get a contradiction.

Using that the curvature of a multi-valued embedded minimal graph decays faster than quadratically will allow us (as in Theorem I.1.6) to model the graphs  $\Sigma_1, \Sigma_2$  by graphs of harmonic functions. So suppose for a moment that both  $u_1$  and  $u_2$  are harmonic. We will



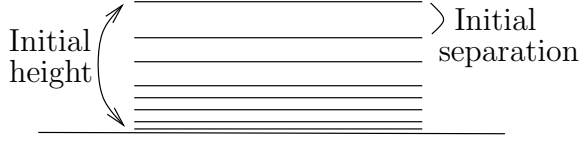


FIGURE 9. The flux argument in the proof of Theorem I.2.1: The initial height and separation.

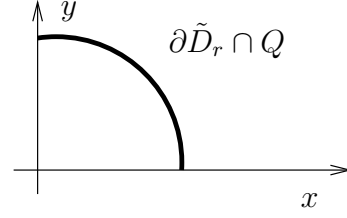


FIGURE 10. The flux argument in the proof of Theorem I.2.1: The curve where the average is calculated over.

show, using a flux argument, that if the separation is large compared with the initial height (see fig. 9), then the fact that the two graphs are part of an embedded minimal disk will eventually force the graphs to grow out of the half-space that they are assumed to lie in. Namely, set

$$\tilde{u}_i(x, y) = u_i(e^x, y) \quad (\text{I.2.2})$$

(i.e., make the conformal change  $\rho = e^x$  and  $\theta = y$ ) and let  $Q$  be the quarter-space  $\{(x, y) \mid x, y \geq 0\}$  and  $\tilde{D}_r = \{(x, y) \mid x^2 + y^2 \leq r^2\}$ . To see that each of the two graphs would grow out of the half-space, set (see fig. 10)

$$\text{Av}_i(r) = \frac{1}{r} \int_{\partial \tilde{D}_r \cap Q} \tilde{u}_i. \quad (\text{I.2.3})$$

The claim follows once we show that there are constants  $C_1$  and  $C_2$  depending on the ratio of the initial height with the initial separation so that for  $r \geq 2$

$$\text{Av}_1(r) + \text{Av}_2(r) - \text{Av}_1(1) - \text{Av}_2(1) \leq -C_1 \log^2 r + C_2 \log r. \quad (\text{I.2.4})$$

Namely, note that if (I.2.4) holds, then the left hand side of (I.2.4) goes to negative infinity as  $r \rightarrow \infty$ , contradicting that each  $\tilde{u}_i > 0$ . Notice that we can take  $r \rightarrow \infty$  to get the contradiction precisely because the radii  $R_i \rightarrow \infty$  in Theorem I.0.5. This is the key place where we use that  $R_i \rightarrow \infty$  (see Part IV for an example which shows this is necessary).

To see (I.2.4), note that when  $u_i$  is harmonic, then so is  $\tilde{u}_i$  and by Stokes' theorem

$$\text{Av}'_i(r) = \frac{1}{r} \int_{\partial \tilde{D}_r \cap Q} \frac{d\tilde{u}_i}{dn} = \frac{1}{r} \int_0^r \frac{\partial \tilde{u}_i}{\partial y}(s, 0) ds + \frac{1}{r} \int_0^r \frac{\partial \tilde{u}_i}{\partial x}(0, s) ds. \quad (\text{I.2.5})$$

Using that the separation is roughly equal to  $2\pi(u_i)_\theta$  we get by combining (I.2.5) with the lower bound for the separation from Theorem I.1.6 that (more or less)

$$\text{Av}'_i(r) \leq -\frac{C_1 \log r}{2r} + \frac{1}{r} \int_0^r \frac{\partial \tilde{u}_i}{\partial x}(0, s) ds. \quad (\text{I.2.6})$$

Since the two spiraling curves (i.e.,  $\theta \rightarrow (\theta, u_i(1, \theta))$  for  $i = 1, 2$ , see fig. 11) together with the two short curves that are assumed to exist bounds a disk (see fig. 12), we get by Stokes' theorem (see lemma 5.1 of [CM8]) that

$$\left| \int_0^r \frac{\partial \tilde{u}_1}{\partial x}(0, s) ds + \int_0^r \frac{\partial \tilde{u}_2}{\partial x}(0, s) ds \right| = \left| \int_0^r \frac{\partial u_1}{\partial \rho}(1, \theta) d\theta + \int_0^r \frac{\partial u_2}{\partial \rho}(1, \theta) d\theta \right| \leq C_2. \quad (\text{I.2.7})$$

Here, we bounded the flux along the short curves by the length of the curves since each  $|\nabla u_i| \leq 1$  (as is the case for the restrictions of the coordinate functions). Adding the bounds on  $Av'_1$  and  $Av'_2$  in (I.2.6) and substituting (I.2.7) gives

$$Av'_1(r) + Av'_2(r) \leq -\frac{C_1 \log r}{r} + \frac{C_2}{r}. \quad (\text{I.2.8})$$

Integrating (I.2.8) gives (I.2.4).

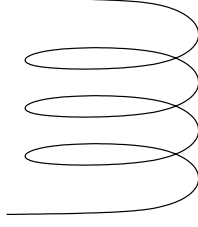


FIGURE 11. The flux argument in the proof of Theorem I.2.1: One of the two spiraling curves;  $\theta \rightarrow (\theta, u_i(1, \theta))$ .

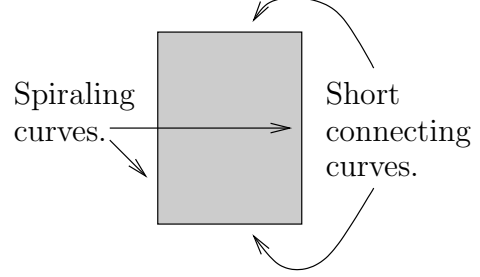


FIGURE 12. The flux argument in the proof of Theorem I.2.1: The two short curves together with the two spiraling curves bounds a disk in  $\Sigma$ .

In the general case where  $u_i$  satisfies the minimal surface equation there are a number of difficulties that have to be dealt with; see lemma 4.1 of [CM8].

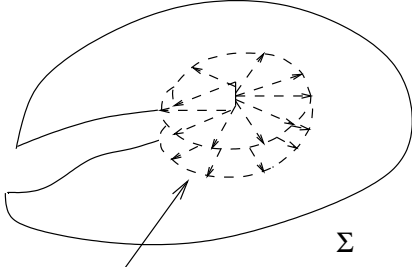
Now this was a little analysis of multi-valued solutions of the minimal surface equation and can all be found in [CM8]. It illustrates that once we show existence of multi-valued minimal graphs in embedded minimal disks and know that such graphs extend as graphs with a sufficiently rapidly growing number of sheets, then we get a removable singularity theorem.

### I.3. EXISTENCE OF MULTI-VALUED GRAPHS AND THE ONE-SIDED CURVATURE ESTIMATE

We now come to our key results for embedded minimal disks. These are some of the main ingredients in the proof of Theorem I.0.5. The first says that if the curvature of such a disk  $\Sigma$  is large at some point  $x \in \Sigma$ , then nearby  $x$  a multi-valued graph forms (in  $\Sigma$ ) and this extends (in  $\Sigma$ ) almost all the way to the boundary. Precisely this is:

**Theorem I.3.1.** (Theorem 0.2 in [CM4]). See fig. 13 and fig. 14. Given  $N \in \mathbf{Z}_+$ ,  $\epsilon > 0$ , there exist  $C_1, C_2 > 0$  so: Let  $0 \in \Sigma \subset B_R \subset \mathbf{R}^3$  be an embedded minimal disk,  $\partial\Sigma \subset \partial B_R$ . If  $\max_{B_{r_0} \cap \Sigma} |A|^2 \geq 4C_1^2 r_0^{-2}$  for some  $R > r_0 > 0$ , then there exists (after a rotation) an  $N$ -valued graph  $\Sigma_g \subset \Sigma$  over  $D_{R/C_2} \setminus D_{2r_0}$  with gradient  $\leq \epsilon$  and  $\Sigma_g \subset \{x_3^2 \leq \epsilon^2(x_1^2 + x_2^2)\}$ .

As a consequence of Theorem I.3.1, one easily gets that if  $|A|^2$  is blowing up near 0 for a sequence of embedded minimal disks  $\Sigma_i$ , then there is a sequence of 2-valued graphs  $\Sigma_{i,d} \subset \Sigma_i$ , where the 2-valued graphs start off on a smaller and smaller scale (namely,  $r_0$  in Theorem I.3.1 can be taken to be smaller as the curvature gets larger). Consequently, by the sublinear separation growth, such 2-valued graphs collapse and, hence, a subsequence



Small multi-valued graph near 0.

FIGURE 13. Part 1 of the proof of Theorem I.3.1; see Theorem II.0.14 - finding a small multi-valued graph in a disk near a point of large curvature.

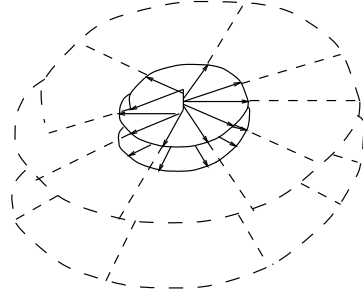


FIGURE 14. Part 2 of the proof of Theorem I.3.1; see Theorem II.0.16 - extending a small multi-valued graph in a disk.

converges to a smooth minimal graph through 0. To be precise, given any fixed  $\rho > 0$ , (I.1.2) bounds the separation  $w$  at  $(\rho, 0)$  by

$$|w(\rho, 0)| \leq \left(\frac{\rho}{r_0}\right)^\alpha |w(r_0, 0)| \leq 2\pi \epsilon \rho^\alpha r_0^{1-\alpha}, \quad (\text{I.3.2})$$

and this goes to 0 as  $r_0 \rightarrow 0$  since  $\alpha < 1$ . The bound  $|w(r_0, 0)| \leq 2\pi \epsilon r_0$  in (I.3.2) came from integrating the gradient bound on the graph around the circle of radius  $r_0$ . (Here 0 is a removable singularity for the limit.) Moreover, if the sequence of such disks is as in Theorem I.0.5, i.e., if  $R_i \rightarrow \infty$ , then the minimal graph in the limit is entire and hence, by Bernstein's theorem (theorem 1.16 in [CM1]), is a plane.

The second key result is the curvature estimate for embedded minimal disks in a half-space. This theorem says roughly that if an embedded minimal disk lies in a half-space above a plane and comes close to the plane, then it is a graph over the plane. Precisely, this is the following theorem:

**Theorem I.3.3.** (Theorem 0.2 in [CM6]). See fig. 15. There exists  $\epsilon > 0$ , such that if  $\Sigma \subset B_{2r_0} \cap \{x_3 > 0\} \subset \mathbf{R}^3$  is an embedded minimal disk with  $\partial\Sigma \subset \partial B_{2r_0}$ , then for all components  $\Sigma'$  of  $B_{r_0} \cap \Sigma$  which intersect  $B_{\epsilon r_0}$

$$\sup_{\Sigma'} |A_\Sigma|^2 \leq r_0^{-2}. \quad (\text{I.3.4})$$

Using the minimal surface equation and that  $\Sigma'$  has points close to a plane, it is not hard to see that, for  $\epsilon > 0$  sufficiently small, (I.3.4) is equivalent to the statement that  $\Sigma'$  is a graph over the plane  $\{x_3 = 0\}$ .

An embedded minimal surface  $\Sigma$  which is as in Theorem I.3.3 is said to satisfy the  $(\epsilon, r_0)$ -effective one-sided Reifenberg condition; cf. appendix A of [CM6] and the appendix of [ChC]. We will often refer to Theorem I.3.3 as *the one-sided curvature estimate*.

Note that the assumption in Theorem I.3.3 that  $\Sigma$  is simply connected is crucial as can be seen from the example of a rescaled catenoid. The catenoid is the minimal surface in  $\mathbf{R}^3$  given by  $(\cosh s \cos t, \cosh s \sin t, s)$  where  $s, t \in \mathbf{R}$ ; see fig. 16. Under rescalings this converges (with multiplicity two) to the flat plane; see fig. 17. Likewise, by considering the

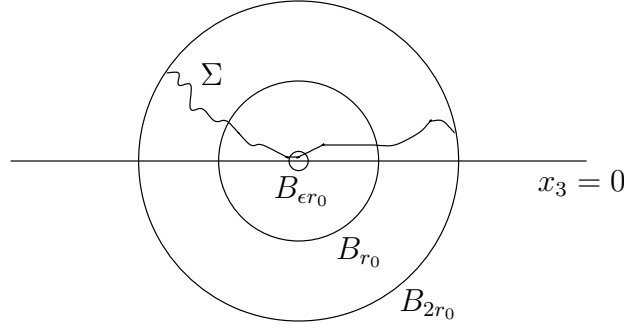


FIGURE 15. Theorem I.3.3 - the one-sided curvature estimate for an embedded minimal disk  $\Sigma$  in a half-space with  $\partial\Sigma \subset \partial B_{2r_0}$ : The components of  $B_{r_0} \cap \Sigma$  intersecting  $B_{\epsilon r_0}$  are graphs.

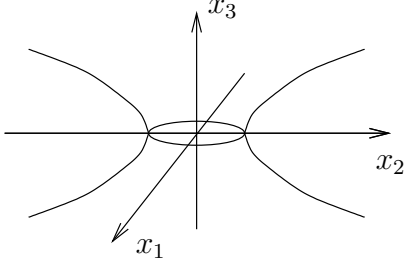


FIGURE 16. The catenoid given by revolving  $x_1 = \cosh x_3$  around the  $x_3$ -axis.

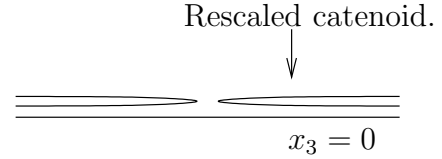


FIGURE 17. Rescaling the catenoid shows that simply connected (and embedded) is needed in the one-sided curvature estimate.

universal cover of the catenoid, one sees that embedded, and not just immersed, is needed in Theorem I.3.3.

As an almost immediate consequence of Theorem I.3.3 and a simple barrier argument we get that if in a ball two embedded minimal disks come close to each other near the center of the ball then each of the disks are graphs. Precisely, this is the following:

**Corollary I.3.5.** (Corollary 0.4 in [CM6]). See fig. 18. There exist  $c > 1$ ,  $\epsilon > 0$  so: Let  $\Sigma_1, \Sigma_2 \subset B_{cr_0} \subset \mathbf{R}^3$  be disjoint embedded minimal surfaces with  $\partial\Sigma_i \subset \partial B_{cr_0}$  and  $B_{\epsilon r_0} \cap \Sigma_i \neq \emptyset$ . If  $\Sigma_1$  is a disk, then for all components  $\Sigma'_1$  of  $B_{r_0} \cap \Sigma_1$  which intersect  $B_{\epsilon r_0}$

$$\sup_{\Sigma'_1} |A|^2 \leq r_0^{-2}. \quad (\text{I.3.6})$$

Theorem I.3.3 is used to show that the points of large curvature in an embedded minimal disk all lie on a Lipschitz curve. To be able to discuss this and explain why this follows from the theorem lets introduce some notation for cones.

If  $\delta > 0$  and  $z \in \mathbf{R}^3$ , then we denote by  $\mathbf{C}_\delta(z)$  the (convex) cone with vertex  $z$ , cone angle  $(\pi/2 - \arctan \delta)$ , and axis parallel to the  $x_3$ -axis. That is, see fig. 19,

$$\mathbf{C}_\delta(z) = \{x \in \mathbf{R}^3 \mid x_3^2 \geq \delta^2 (x_1^2 + x_2^2)\} + z. \quad (\text{I.3.7})$$

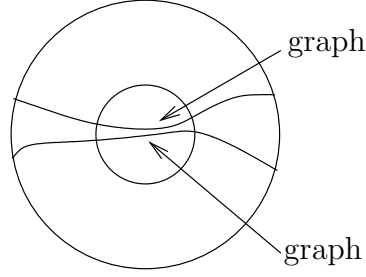


FIGURE 18. Corollary I.3.5: Two sufficiently close components of an embedded minimal disk must each be a graph.

The next direct consequence of Theorem I.3.3 (with  $\Sigma_d$  playing the role of the plane  $x_3 = 0$ ) will be needed when we sketch the proof of Theorem I.0.5 in the next section. This consequence says that the points of large curvature in an embedded minimal disk have what we will in the next section call the cone property. Namely, given a point of large curvature in such a disk, the next corollary asserts that all the other points of large curvature lie within a double convex cone with vertex at the initial point of large curvature. This is the result that will eventually give the regularity of the singular set (the set of points of large curvature). Precisely, this consequence of Theorem I.3.3 is the following:

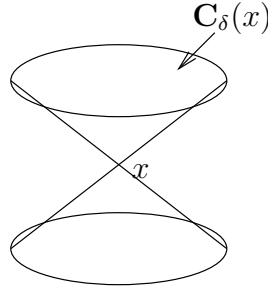


FIGURE 19. The cone  $\mathbf{C}_\delta(x)$ .

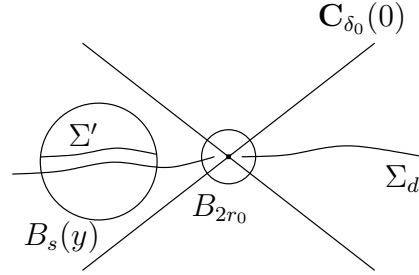


FIGURE 20. Corollary I.3.8: With  $\Sigma_d$  playing the role of  $x_3 = 0$ , by the one-sided estimate,  $\Sigma$  consists of multi-valued graphs away from a cone.

**Corollary I.3.8.** (Corollary I.1.9 in [CM6]). See fig. 20. There exists  $\delta_0 > 0$  so: Suppose  $\Sigma \subset B_{2R}$ ,  $\partial\Sigma \subset \partial B_{2R}$  is an embedded minimal disk containing a 2-valued graph  $\Sigma_d \subset \{x_3^2 \leq \delta_0^2(x_1^2 + x_2^2)\}$  over  $D_R \setminus D_{r_0}$  with gradient  $\leq \delta_0$ . Then each component of  $B_{R/2} \cap \Sigma \setminus (\mathbf{C}_{\delta_0}(0) \cup B_{2r_0})$  is a multi-valued graph with gradient  $\leq 1$ .

Fig. 20 illustrates how this corollary follows from Theorem I.3.3. In this picture,  $B_s(y)$  is a ball away from 0 and  $\Sigma'$  is a component of  $B_s(y) \cap \Sigma$  disjoint from  $\Sigma_d$ . It follows easily from the maximum principle that  $\Sigma'$  is topologically a disk. Since  $\Sigma'$  is assumed to contain points near  $\Sigma_d$ , then we can let a component of  $B_s(y) \cap \Sigma_d$  play the role of the plane  $\{x_3 = 0\}$  in Theorem I.3.3 and the corollary follows.

Note that, since  $\Sigma$  is compact and embedded, the multi-valued graphs given by Corollary I.3.8 spiral through the cone. Namely, if a graph did close up, then the graph containing  $\Sigma_d$  would be forced to accumulate into it, contradicting compactness.

It can also be seen from Corollary I.3.8 (see corollary 6.3 of [CM8]) that if  $\Sigma_d$  and  $\Sigma$  are as in Corollary I.3.8, then  $\Sigma_d$  extends in  $\Sigma \setminus \mathbf{C}_{\delta_0}(0)$  to a multi-valued graph with at least  $(\log \rho)^2$  many sheets. Thus Theorem I.1.6 applies.

#### I.4. REGULARITY OF THE SINGULAR SET AND THEOREM I.0.5

In this section we will indicate how to define the singular set  $\mathcal{S}$  in Theorem I.0.5 and show the regularity of  $\mathcal{S}$ .

First, by a very general compactness argument, we have that for any sequence of surfaces in  $\mathbf{R}^3$  (minimal or not), after possibly going to a subsequence, then there is a well defined notion of points where the second fundamental form of the sequence blows up.

**Lemma I.4.1.** Let  $\Sigma_i \subset B_{R_i}$ ,  $\partial \Sigma_i \subset \partial B_{R_i}$ , and  $R_i \rightarrow \infty$  be a sequence of (smooth) compact surfaces. After passing to a subsequence,  $\Sigma_j$ , we may assume that for each  $x \in \mathbf{R}^3$  either (a) or (b) holds:

- (a)  $\sup_{B_r(x) \cap \Sigma_j} |A|^2 \rightarrow \infty$  for all  $r > 0$ ,
- (b)  $\sup_j \sup_{B_r(x) \cap \Sigma_j} |A|^2 < \infty$  for some  $r > 0$ .

*Proof.* For  $r > 0$  and an integer  $n$ , define a sequence of functions on  $\mathbf{R}^3$  by

$$\mathcal{A}_{i,r,n}(x) = \min\{n, \sup_{B_r(x) \cap \Sigma_i} |A|^2\}, \quad (\text{I.4.2})$$

where we set  $\sup_{B_r(x) \cap \Sigma_i} |A|^2 = 0$  if  $B_r(x) \cap \Sigma_i = \emptyset$ . Set

$$\mathcal{D}_{i,r,n} = \lim_{k \rightarrow \infty} 2^{-k} \sum_{m=0}^{2^k-1} \mathcal{A}_{i,(1+m2^{-k})r,n}, \quad (\text{I.4.3})$$

then  $\mathcal{D}_{i,r,n}$  is continuous and  $\mathcal{A}_{i,2r,n} \geq \mathcal{D}_{i,r,n} \geq \mathcal{A}_{i,r,n}$ . Let  $\nu_{i,r,n}$  be the (bounded) functionals,

$$\nu_{i,r,n}(\phi) = \int_{B_n} \phi \mathcal{D}_{i,r,n} \text{ for } \phi \in L^2(\mathbf{R}^3). \quad (\text{I.4.4})$$

By standard compactness for fixed  $r, n$ , after passing to a subsequence,  $\nu_{j,r,n} \rightarrow \nu_{r,n}$  weakly. In fact (since the unit ball in  $L^2(\mathbf{R}^3)$  has a countable basis), by an easy diagonal argument, after passing to a subsequence, we may assume that for all  $n, m \geq 1$  fixed  $\nu_{j,2^{-m},n} \rightarrow \nu_{2^{-m},n}$  weakly. Note that if  $x \in \mathbf{R}^3$  and for all  $m, n$  with  $n \geq |x| + 1$ , (identify  $B_{2^{-m}}(x)$  with its characteristic function)

$$\nu_{2^{-m},n}(B_{2^{-m}}(x)) \geq n \text{ Vol}(B_{2^{-m}}), \quad (\text{I.4.5})$$

then for each fixed  $r > 0$ ,  $\sup_{B_r(x) \cap \Sigma_j} |A|^2 \rightarrow \infty$ . Conversely, if for some  $n \geq |x| + 1$ ,  $m$ , (I.4.5) fails at  $x$ , then  $\sup_j \sup_{B_r(x) \cap \Sigma_j} |A|^2 < \infty$  for  $r = 2^{-m-1}$ .  $\square$

From this lemma we have that after possibly passing to a subsequence, then there is a well defined notion of the set of points where the curvatures blow up of a given sequence of embedded minimal disks. To show that this set is in fact a Lipschitz curve we will see below

that, as a consequence of the one sided curvature estimate, the set of such points has what we will call the cone property.

Fix  $\delta > 0$ . We will say that a subset  $\mathcal{S} \subset \mathbf{R}^3$  has the cone property (or the  $\delta$ -cone property) if  $\mathcal{S}$  is closed and nonempty and the following holds:

- (1) If  $z \in \mathcal{S}$ , then  $\mathcal{S} \subset \mathbf{C}_\delta(z)$ .
- (2) If  $t \in x_3(\mathcal{S})$  and  $\epsilon > 0$ , then  $\mathcal{S} \cap \{t < x_3 < t + \epsilon\} \neq \emptyset$  and  $\mathcal{S} \cap \{t - \epsilon < x_3 < t\} \neq \emptyset$ .

Note that (2) just says that each point in  $\mathcal{S}$  is the limit of points coming from above and below.

When  $\Sigma_i \subset B_{R_i} \subset \mathbf{R}^3$  is a sequence of embedded minimal disks with  $\partial\Sigma \subset \partial B_{R_i}$ ,  $R_i \rightarrow \infty$  and  $\Sigma_j$  is the subsequence given by Lemma I.4.1 and  $\mathcal{S}$  is the sets of points where the curvatures of  $\Sigma_j$  blow up (i.e., where (a) in Lemma I.4.1 holds), then (as we indicated above) we will see below that  $\mathcal{S}$  has the cone property (after a rotation of  $\mathbf{R}^3$ ). Hence (by the next lemma),  $\mathcal{S}$  is in this case a Lipschitz curve which is a graph over the  $x_3$ -axis. Note that in the case where  $\Sigma_i$  is a sequence of rescaled helicoids, then  $\mathcal{S}$  is simply the  $x_3$ -axis.

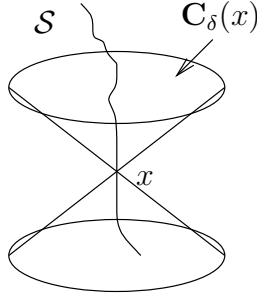


FIGURE 21. It follows from the one-sided curvature estimate that the singular set has the cone property and hence is a Lipschitz curve.

**Lemma I.4.6.** See fig. 21. If  $\mathcal{S} \subset \mathbf{R}^3$  has the  $\delta$ -cone property, then  $\mathcal{S} \cap \{x_3 = t\}$  consists of exactly one point  $\mathcal{S}_t$  for all  $t \in \mathbf{R}$ , and  $t \rightarrow \mathcal{S}_t$  is a Lipschitz parameterization of  $\mathcal{S}$  with

$$|t_2 - t_1| \leq |\mathcal{S}_{t_2} - \mathcal{S}_{t_1}| \leq \sqrt{1 + \delta^{-2}} |t_2 - t_1|. \quad (\text{I.4.7})$$

*Proof.* Since  $\mathcal{S}$  is nonempty, we may after translation assume that  $0 \in \mathcal{S}$ . By (1), it follows that  $\mathcal{S} \cap \{x_3 = t\}$  consists of at most one point for each  $t \in \mathbf{R}$ . Assume that  $\mathcal{S} \cap \{x_3 = t_0\} = \emptyset$  for some  $t_0$ . Since  $\mathcal{S} \subset \mathbf{R}^3$  is a nonempty closed set and  $x_3 : \mathcal{S} \subset \mathbf{C}_\delta(0) \rightarrow \mathbf{R}$  is proper, then  $x_3(\mathcal{S}) \subset \mathbf{R}$  is also closed (and nonempty). Let  $t_s \in x_3(\mathcal{S})$  be the closest point in  $x_3(\mathcal{S})$  to  $t_0$ . The desired contradiction now easily follows since either  $\mathcal{S} \cap \{t_s < x_3 < t_0\}$  or  $\mathcal{S} \cap \{t_0 < x_3 < t_s\}$  is nonempty by assumption.

It follows that  $t \rightarrow \mathcal{S}_t$  is a well-defined curve (from  $\mathbf{R}$  to  $\mathcal{S}$ ). Moreover, since

$$\mathcal{S}_{t_2} \subset \{x_3 = t_1 + (t_2 - t_1)\} \cap \mathbf{C}_\delta(\mathcal{S}_{t_1}) \subset B_{\sqrt{1+\delta^{-2}}|t_2-t_1|}(\mathcal{S}_{t_1}), \quad (\text{I.4.8})$$

(I.4.7) follows.  $\square$

Suppose next that  $\Sigma_i$  is as in Theorem I.0.5, that is,  $\Sigma_i \subset B_{R_i} = B_{R_i}(0) \subset \mathbf{R}^3$  is a sequence of embedded minimal disks with  $\partial\Sigma_i \subset \partial B_{R_i}$  where  $R_i \rightarrow \infty$  and  $\sup_{B_1 \cap \Sigma_i} |A|^2 \rightarrow \infty$ . Let



$\Sigma_j$  and  $\mathcal{S}$  be the subsequence and set, respectively, given by Lemma I.4.1 ( $\mathcal{S}$  is the set of points where (a) holds in Lemma I.4.1). In particular,  $\mathcal{S}$  is closed by definition and nonempty by the assumption of Theorem I.0.5. From Corollary I.3.8 (cf. the sketch of the proof of Theorem I.0.5 below), it follows that (1) above holds, so to see that  $\mathcal{S}$  has the cone property all we need to see is that (2) holds. This follows from the next lemma which relies in part on Theorem I.2.1:

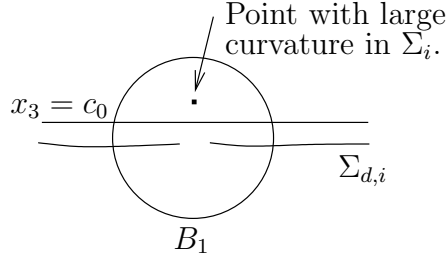


FIGURE 22. Lemma I.4.9 - points with large curvature in  $\Sigma_i$  above the plane  $x_3 = c_0$  but near the center of the 2-valued graphs  $\Sigma_{d,i}$ .

**Lemma I.4.9.** (Lemma I.1.10 in [CM6]). See fig. 22. There exists  $c_0 > 0$  so: Let  $\Sigma_i \subset B_{R_i}$ ,  $\partial\Sigma_i \subset \partial B_{R_i}$  be a sequence of embedded minimal disks with  $R_i \rightarrow \infty$ . If  $\Sigma_{d,i} \subset \Sigma_i$  is a sequence of 2-valued graphs over  $D_{R_i/C} \setminus D_{\epsilon_i}$  with  $\epsilon_i \rightarrow 0$  and  $\Sigma_{d,i} \rightarrow \{x_3 = 0\} \setminus \{0\}$ , then

$$\sup_{B_1 \cap \Sigma_i \cap \{x_3 > c_0\}} |A|^2 \rightarrow \infty. \quad (\text{I.4.10})$$

**Sketch of the proof of Theorem I.0.5:** From all of these results above, we know that if  $\Sigma_i$  is a sequence as in Theorem I.0.5 and  $\Sigma_j$ ,  $\mathcal{S}$  are given by Lemma I.4.1, then  $\mathcal{S}$  has the cone property and hence, by Lemma I.4.1,  $\mathcal{S}$  is a Lipschitz graph over the  $x_3$ -axis. As mentioned above, it also follows from Theorem I.3.1 together with Bernstein's theorem that, for each  $x \in \mathcal{S}$  and each  $j$  sufficiently large, there is a 2-valued graph in  $\Sigma_j$  and that this sequence of 2-valued graphs converges (after possibly going to a subsequence) to a plane through  $x$ . Since  $\Sigma_j$  is embedded, all of these planes coming from different points  $x \in \mathcal{S}$  must be parallel and it now follows from the one sided curvature estimate that  $\Sigma_j$  consists of multi-valued graphs away from  $\mathcal{S}$ . It is easy to see that there must be at least two such multi-valued graphs in the complement of  $\mathcal{S}$ . That there are not more than two follows from a barrier argument; see proposition II.1.3 of [CM6]. This completes the rough sketch of the proof of Theorem I.0.5.

## Part II. The proof of the existence of multi-valued graphs

Before we proceed let us briefly review the strategy of the proof of our main theorem that every embedded minimal disk is either a graph of a function or part of a double spiral staircase.

The proof has the following three main steps; see fig. 23:

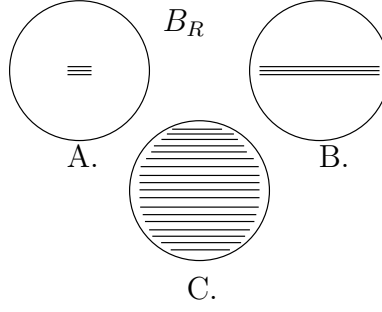


FIGURE 23. Proving Theorem I.0.5.  
 A. Finding a small  $N$ -valued graph in  $\Sigma$ . B. Extending it in  $\Sigma$  to a large  $N$ -valued graph. C. Extending the number of sheets.

A. Fix an integer  $N$  (the “large” of the curvature in what follows will depend on  $N$ ). If an embedded minimal disk  $\Sigma$  is not a graph (or equivalently if the curvature is large at some point), then it contains an  $N$ -valued minimal graph which initially is shown to exist on the scale of  $1/\max|A|$ . That is, the  $N$ -valued graph is initially shown to be defined on an annulus with both inner and outer radius inversely proportional to  $\max|A|$ .

B. Such a potentially small  $N$ -valued graph sitting inside  $\Sigma$  can then be seen to extend as an  $N$ -valued graph inside  $\Sigma$  almost all the way to the boundary. That is, the small  $N$ -valued graph can be extended to an  $N$ -valued graph defined on an annulus where the outer radius of the annulus is proportional to  $R$ . Here  $R$  is the radius of the ball in  $\mathbf{R}^3$  that the boundary of  $\Sigma$  is contained in.

C. The  $N$ -valued graph not only extends horizontally (i.e., tangent to the initial sheets) but also vertically (i.e., transversally to the sheets). That is, once there are  $N$  sheets there are many more and, in fact, the disk  $\Sigma$  consists of two multi-valued graphs glued together along an axis.

To describe the existence, i.e., A., of multi-valued graphs in embedded minimal disks, we will need the notion of a blow up point. Roughly speaking, a blow up point is a point where the curvature is, up to a fixed constant, the maximum.

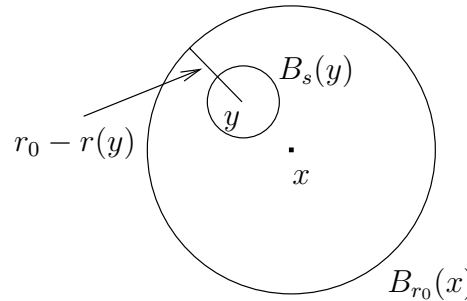


FIGURE 24. Existence of blow up points, that is pairs of points  $y \in \Sigma$  and  $s > 0$  satisfying (II.0.11).

To make this precise, let  $x \in \Sigma \subset B_{r_0}(x) \subset \mathbf{R}^3$  be a smooth (compact) surface embedded, or just immersed, with  $\partial\Sigma \subset \partial B_{r_0}(x)$ . Here  $B_{r_0}(x)$  is the extrinsic ball of radius  $r_0$  but could as well have been an intrinsic ball in which case the notion of a blow up point below would have to be appropriately changed. Suppose that  $|A|^2(x) \geq 4C^2 r_0^{-2}$  for some constant  $C > 0$ . We claim that there is a “blow up point”  $y \in B_{r_0}(x) \cap \Sigma$  and  $s > 0$  such that  $B_s(y) \subset B_{r_0}(x)$  and

$$\sup_{B_s(y) \cap \Sigma} |A|^2 \leq 4C^2 s^{-2} = 4|A|^2(y). \quad (\text{II.0.11})$$

That is, the curvature at  $y$  is large (this just means that  $C$  should be thought of as a large constant) and is almost (up to the constant 4) the maximum on the ball  $B_s(y)$ .

*Proof.* (of claim) That there exists such a point  $y$  is easy to see; on  $B_{r_0}(x) \cap \Sigma$  set  $F(z) = (r_0 - r(z))^2 |A|^2(z)$  where  $r(z) = |z - x|$ . Then

$$F(x) \geq 4C^2, F \geq 0, \text{ and } F|_{\partial B_{r_0}(x) \cap \Sigma} = 0. \quad (\text{II.0.12})$$

Let  $y$  be where the maximum of  $F$  is achieved and set  $s = C/|A|(y)$ . One easily checks that  $y, s$  have the required properties; see fig. 24. Namely, clearly  $|A|^2(y) = C^2 s^{-2}$  and since  $y$  is where the maximum of  $F$  is achieved,

$$|A|^2(z) \leq \left( \frac{r_0 - r(y)}{r_0 - r(z)} \right)^2 |A|^2(y). \quad (\text{II.0.13})$$

Since  $F(x) \geq 4C^2$  it follows from the choice of  $s$  that  $|r_0 - r(y)| \leq 2|r_0 - r(z)|$  for  $z \in B_s(y) \cap \Sigma$ . Hence,  $|A|^2(z) \leq 4|A|^2(y)$ . Together this gives (II.0.11).  $\square$

Returning to the existence of multi-valued graphs, then the way we showed Theorem I.3.1 was by combining a blow up result with the extension of multi-valued graphs proven in [CM3]. This blow up result says that if an embedded minimal disk in a ball has large curvature at a point, then it contains a small (in fact on the scale of one over the square root of the curvature) almost flat multi-valued graph nearby, that is:

**Theorem II.0.14.** (Theorem 0.4 in [CM4]). See fig. 13. Given  $N, \omega > 1$ , and  $\epsilon > 0$ , there exists  $C = C(N, \omega, \epsilon) > 0$  so: Let  $0 \in \Sigma \subset B_R \subset \mathbf{R}^3$  be an embedded minimal disk,  $\partial\Sigma \subset \partial B_R$ . If  $\sup_{B_{r_0} \cap \Sigma} |A|^2 \leq 4C^2 r_0^{-2} = 4|A|^2(0)$  for some  $0 < r_0 < R$ , then there exist  $\bar{R} < r_0/\omega$  and (after a rotation) an  $N$ -valued graph  $\Sigma_g \subset \Sigma$  over  $D_{\omega\bar{R}} \setminus D_{\bar{R}}$  with gradient  $\leq \epsilon$ , and  $\text{dist}_\Sigma(0, \Sigma_g) \leq 4\bar{R}$ .

Note that 0 in Theorem II.0.14 is a blow up point in the above sense.

The result that we needed from [CM3] (combining theorem 0.3 and lemma II.3.8 there) is Theorem II.0.16 below that allows us to extend the (small) multi-valued graphs given by Theorem II.0.14 almost out to the boundary of the “big” ball  $B_R$ . In this theorem, by the middle sheet  $(\Sigma_g)^M$  of an  $N$ -valued graph  $\Sigma_g$  we mean the portion over

$$\{(\rho, \theta) \in \mathcal{P} \mid r_1 < \rho < r_2 \text{ and } 0 \leq \theta \leq 2\pi\}. \quad (\text{II.0.15})$$

**Theorem II.0.16.** [CM3]. See fig. 14. Given  $N_1$  and  $\tau > 0$ , there exist  $N, \Omega, \epsilon > 0$  so: If  $\Omega r_0 < 1 < R/\Omega$ ,  $\Sigma \subset B_R$  is an embedded minimal disk with  $\partial\Sigma \subset \partial B_R$ , and  $\Sigma$  contains an  $N$ -valued minimal graph  $\Sigma_g$  over  $D_1 \setminus D_{r_0}$  with gradient  $\leq \epsilon$  and  $\Sigma_g \subset \{x_3^2 \leq \epsilon^2(x_1^2 + x_2^2)\}$ , then  $\Sigma$  contains a  $N_1$ -valued graph  $\Sigma_d$  over  $D_{R/\Omega} \setminus D_{r_0}$  with gradient  $\leq \tau$  and  $(\Sigma_g)^M \subset \Sigma_d$ .

## II.1. THE PROOF OF EXISTENCE OF SMALL MULTI-VALUED GRAPHS - THEOREM II.0.14

We will here describe some of the ideas that go into the proof of the existence of the small multi-valued graphs near a point of large curvature. That is, the proof of Theorem II.0.14. In this theorem,  $\Sigma$  is an embedded minimal disk and  $0 \in \Sigma$  is a blow up point with scale  $r_0$  satisfying

$$\sup_{B_{r_0} \cap \Sigma} |A|^2 \leq 4 C^2 r_0^{-2} = 4 |A|^2(0). \quad (\text{II.1.1})$$

The theorem then gives a multi-valued graph  $\Sigma_g$  contained in  $\Sigma$  defined on the scale  $r_0$  ((II.1.1) says that  $r_0$  is proportional to one over the squareroot of the curvature)

The key step in finding the multi-valued graph is to find many large pieces of  $\Sigma$  with a (scale-invariant) quadratic curvature bound (these pieces will be intrinsic sectors; see fig. 27). To do this, we use the upper bound on  $|A|^2$  in (II.1.1) to prove that the area of intrinsic balls in  $\Sigma$  grows polynomially and, consequently, get an average curvature bound. This average curvature bound and a curvature estimate for embedded disks (see Proposition II.1.5 below) will give large pieces of  $\Sigma$  with the desired quadratic curvature bound. Using the lower bound on  $|A|^2(0)$  in (II.1.1), we show that there are many such pieces so that two must be close together in  $\mathbf{R}^3$ ; embeddedness implies that these are disjoint, hence almost stable, and therefore nearly flat. Piecing together these large flat pieces then gives the desired  $N$ -valued graph.

Throughout this section,  $\Sigma \subset B_R$  is an embedded minimal disk with  $\partial\Sigma \subset \partial B_R$ .

Before discussing the main steps in the proof, we will need to recall three facts about minimal surfaces from [CM4]. The first is the relationship between area and total curvature of intrinsic balls for disks with nonpositive curvature. The second is a curvature estimate for embedded minimal disks with bounded total curvature. The third is that nearby, but disjoint, minimal surfaces with bounded curvature must in fact be almost stable.

Area and total curvature. The relationship between area and total curvature is particularly simple for disks. Essentially, this is because the first variation of length of a geodesic circle is (up to a constant) given by the total curvature of the disk using the Gauss-Bonnet theorem; this can also be seen using the Jacobi equation for geodesics. Namely, as in corollary 1.7 of [CM4], integrating the Jacobi equation (for geodesics) and using  $K_\Sigma = -|A|^2/2$  gives

$$4 (\text{Area}(\mathcal{B}_R) - \pi R^2) = 2 \int_0^R \int_0^t \int_{\mathcal{B}_s} |A|^2 = \int_{\mathcal{B}_R} |A|^2 (R - r)^2, \quad (\text{II.1.2})$$

where  $r(x) = \text{dist}_\Sigma(0, x)$ . The second equality in (II.1.2) used two integrations by parts (i.e.,  $\int_0^R f(t) g''(t) dt = \int_0^R f''(t) g(t) dt$  with  $f(t) = \int_0^t \int_{\mathcal{B}_s} |A|^2$  and  $g(t) = (R - t)^2$ ).

We will see that (II.1.2) often leads to bounds on the area of the ball  $\mathcal{B}_R$ . For example, when  $\mathcal{B}_R$  is stable, then using  $R - r$  (which vanishes on  $\partial\mathcal{B}_R$ ) in the stability inequality (see (II.1.9) below) gives

$$4 (\text{Area}(\mathcal{B}_R) - \pi R^2) = \int_{\mathcal{B}_R} |A|^2 (R - r)^2 \leq \int_{\mathcal{B}_R} |\nabla(R - r)|^2 = \text{Area}(\mathcal{B}_R). \quad (\text{II.1.3})$$

Consequently, we get an a priori bound for the area of an intrinsic ball in a stable minimal disk

$$\text{Area}(\mathcal{B}_R) \leq 4\pi R^2/3. \quad (\text{II.1.4})$$

(This area bound is the starting point in [CM2].) We will use two generalizations of this argument below. The first will get a polynomial area bound for embedded minimal disks with bounded curvature. The second generalization will be to bound the area of a 1/2-stable sector (a sector is a specific type of subdomain of an intrinsic ball).

A curvature estimate for embedded disks with bounded total curvature. The following curvature estimate for embedded minimal disks  $\Sigma$  generalizes a result of Schoen and Simon (theorem 2.5 in [CM1]):

**Proposition II.1.5.** (Corollary 1.18 in [CM4]). Given  $C_I$ , there exists  $C_P$  so that if

$$\int_{\mathcal{B}_{2s}} |A|^2 \leq C_I, \quad (\text{II.1.6})$$

then

$$\sup_{\mathcal{B}_s} |A|^2 \leq C_P s^{-2}. \quad (\text{II.1.7})$$

By (II.1.2), bounds on  $\text{Area}(\mathcal{B}_t)/t^2$ ,  $\text{Length}(\partial\mathcal{B}_t)/t$ , or  $\int_{\mathcal{B}_t} |A|^2$  are equivalent (if we are willing to go to subballs). Therefore, Proposition II.1.5 gives an a priori curvature estimate when any one of these three quantities is bounded. It is important that  $\Sigma$  is an embedded disk; e.g., the catenoid is complete, has finite total curvature, and is not flat.

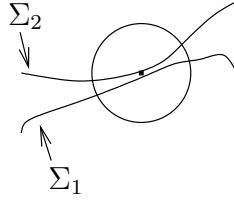


FIGURE 25. Two sufficiently close disjoint minimal surfaces with bounded curvatures must each be nearly stable.

Nearby disjoint surfaces with  $|A|^2 \leq 4$  are nearly stable. See fig. 25. We will see that if two disjoint minimal surfaces with bounded curvature come close enough together, then each of them is 1/2-stable. This 1/2-stability property is a weakening of stability which is still sufficiently strong to imply estimates on the area and curvature of the surfaces.

Before making this precise, recall that the linearization of the minimal graph equation is the Jacobi equation (for minimal surfaces)

$$Lu = \Delta u + |A|^2 u = 0. \quad (\text{II.1.8})$$

A domain  $\Omega \subset \Sigma$  is said to be stable if  $\int \phi L\phi \leq 0$  for every  $\phi$  with compact support in  $\Omega$ ; i.e., if we have the stability inequality

$$\int |A|^2 \phi^2 \leq \int |\nabla \phi|^2. \quad (\text{II.1.9})$$

We will say that  $\Omega$  is 1/2-stable if we have the weaker 1/2-stability inequality

$$\int |A|^2 \phi^2 \leq 2 \int |\nabla \phi|^2. \quad (\text{II.1.10})$$

One useful criterion for stability is that if  $u > 0$  and  $Lu = 0$  on  $\Omega$ , then  $\Omega$  is stable; similarly, when  $u > 0$  and  $Lu/u$  is small, then  $\Omega$  is 1/2-stable (cf. section 2 of [CM4]).

Using the above criteria for stability, we can now explain why nearby, but disjoint, minimal disks with bounded curvature must be 1/2-stable. Namely, if two disjoint minimal disks with  $|A|^2 \leq 4$  come close at a point, then it is not hard to see that one can be written as a (normal exponential) graph over the other of a function  $u > 0$  with  $Lu/u \approx 0$  and, consequently, each is 1/2-stable. This is similar to the case of geodesics. See lemmas 2.6 and 2.11 of [CM4] for the precise statements.

Having these tools at our disposal, we turn next to the main steps in the proof of the existence of the small multi-valued graphs near a point of large curvature.

Polynomial area bounds when  $|A|^2 \leq 4$ . In general, the volume comparison theorem from geometry implies that a surface with bounded curvature has at most exponential area growth (as is the case for hyperbolic space). However, we will see that an embedded minimal disk in  $\mathbf{R}^3$  with bounded curvature actually has polynomial area growth. This will be used to prove a doubling property, that is, to find arbitrarily large balls where the area of the double ball increases by at most a bounded factor (see Corollary II.1.21 below for the precise statement). Notice that this kind of doubling occurs for polynomial growth but not for exponential growth, i.e.,  $\lim_{r \rightarrow \infty} \frac{(2r)^p}{r^p} = 2^p < \infty$  while  $\lim_{r \rightarrow \infty} \frac{e^{2r}}{e^r} = \infty$ .

To get this polynomial area bound, we first show that “most of” an embedded minimal disk  $\Sigma$  with  $|A|^2 \leq 4$  is nearly stable. More precisely, the next lemma decomposes  $\Sigma$  into a union of disjoint 1/2-stable domains  $\Omega_j$  and a remainder with bounded area. Moreover, the lemma also gives a cutoff function with bounded energy which will be used in the 1/2-stability inequality.

**Lemma II.1.11.** (Lemma 2.15 in [CM4]). There exists  $C_1$  so: If  $0 \in \Sigma \subset B_{2R}$ ,  $\partial\Sigma \subset \partial B_{2R}$ , and  $|A|^2 \leq 4$ , then there exist disjoint 1/2-stable subdomains  $\Omega_j \subset \Sigma$  and a function  $\chi \leq 1$  which vanishes on  $B_R \cap \Sigma \setminus \cup_j \Omega_j$  so that

$$\text{Area}(\{x \in B_R \cap \Sigma \mid \chi(x) < 1\}) \leq C_1 R^3, \quad (\text{II.1.12})$$

$$\int_{B_R} |\nabla \chi|^2 \leq C_1 R^3. \quad (\text{II.1.13})$$

*Proof.* (Sketch). Fix  $\rho > 0$  small. Given  $x \in \Sigma$ , let  $\Sigma_x$  be the component of  $B_\rho(x) \cap \Sigma$  with  $x \in \Sigma_x$  and let  $B_x^+$  be the component of  $B_\rho(x) \setminus \Sigma_x$  which  $\mathbf{n}(x)$  points into. Set, see fig. 26,

$$VB = \{x \in B_R \cap \Sigma \mid B_x^+ \cap \Sigma \setminus \mathcal{B}_{4\rho}(x) = \emptyset\} \quad (\text{II.1.14})$$

and let  $\{\Omega_j\}$  be the components of  $B_R \cap \Sigma \setminus \overline{VB}$ . It follows from the previous subsection that each  $\Omega_j$  comes equipped with a positive solution  $u_j$  of the minimal graph equation and is therefore 1/2-stable for  $\rho$  sufficiently small (it is obvious that the function  $u_j$  exists locally, but it requires a slight argument to see that it is globally well-defined).

The function  $\chi$  is a linear cutoff function on the  $\rho$ -tubular neighborhood of  $VB$ , i.e., set

$$\chi(x) = \begin{cases} 0 & \text{if } x \in VB, \\ \text{dist}_\Sigma(x, VB)/\rho & \text{if } 0 \leq \text{dist}(x, VB) \leq \rho, \\ 1 & \text{otherwise.} \end{cases} \quad (\text{II.1.15})$$

Finally, we use a simple ball counting argument to get (II.1.12) and (II.1.13). Roughly speaking, the definition of  $VB$  allows us to cover it by a collection of extrinsic balls  $\{B_{2\rho}(x_i)\}$  so that the “half half-balls”  $B_{x_i}^+$  are essentially disjoint. Since each of these disjoint “half half-balls” has volume  $\approx \rho^3$  and is contained in a fixed ball in  $\mathbf{R}^3$ , there are at most  $C(R/\rho)^3$  such balls. This and the curvature bound easily give (II.1.12) and (II.1.13).  $\square$

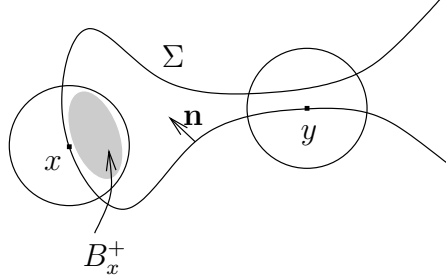


FIGURE 26. The set  $VB$  in (II.1.14):  
 $x \in VB$  and  $y \in \Sigma \setminus VB$ .

Using the decomposition from Lemma II.1.11 in (II.1.2) (as in (II.1.3)) gives polynomial area bounds for intrinsic balls with bounded curvature (Lemma 3.1 in [CM4]):

**Proposition II.1.16.** If  $0 \in \Sigma \subset B_{2R}$ ,  $\partial\Sigma \subset \partial B_{2R}$ , and  $|A|^2 \leq 4$ , then

$$\int_0^R \int_0^t \int_{B_s} |A|^2 ds dt = 2(\text{Area}(\mathcal{B}_R) - \pi R^2) \leq 6\pi R^2 + 20C_1 R^5. \quad (\text{II.1.17})$$

*Proof.* Let the constant  $C_1$ , the function  $\chi$ , and the subdomain  $\cup_j \Omega_j$  be given by Lemma II.1.11. In particular, the function  $\chi(R-r)$  vanishes off of  $\cup_j \Omega_j$ . Using  $\chi(R-r)$  in the 1/2-stability inequality (i.e., in (II.1.10)), the absorbing inequality and (II.1.13) give

$$\begin{aligned} \int |A|^2 \chi^2 (R-r)^2 &\leq 2 \int (\chi^2 + 2\chi R |\nabla \chi| + R^2 |\nabla \chi|^2) \\ &\leq 6R^2 \int_{\mathcal{B}_R} |\nabla \chi|^2 + 3 \int \chi^2 \leq 6C_1 R^5 + 3 \text{Area}(\mathcal{B}_R). \end{aligned} \quad (\text{II.1.18})$$

On the other hand, combining the area bound (II.1.12) for  $\{\chi < 1\}$  and  $|A|^2 \leq 4$  gives

$$\int |A|^2 (1 - \chi^2) (R-r)^2 \leq 4R^2 \text{Area}(\{x \in B_R \cap \Sigma \mid \chi(x) < 1\}) \leq 4C_1 R^5. \quad (\text{II.1.19})$$

We see (II.1.17) by using (II.1.18) and (II.1.19) in (II.1.2) to get

$$4(\text{Area}(\mathcal{B}_R) - \pi R^2) = \int |A|^2 (R-r)^2 \leq 10C_1 R^5 + 3 \text{Area}(\mathcal{B}_R). \quad (\text{II.1.20})$$

$\square$



Using the polynomial area growth proven in Proposition II.1.16, it is now standard to find large intrinsic balls with a fixed doubling for area (and hence also for total curvature by (II.1.2)):

**Corollary II.1.21.** (Corollary 3.5 in [CM4]). There exists  $C_2$  so that given  $\beta, R_0 > 1$ , we get  $R$  so: If  $0 \in \Sigma \subset B_R$  is an embedded minimal disk,  $\partial\Sigma \subset \partial B_R$ ,  $|A|^2(0) = 1$ , and  $|A|^2 \leq 4$ , then there exists  $R_0 \leq s < R/(2\beta)$  with

$$\int_{\mathcal{B}_{3s}} |A|^2 \leq C_2 s^{-2} \text{Area}(\mathcal{B}_s), \quad (\text{II.1.22})$$

$$\beta^{-10} \int_{\mathcal{B}_{2\beta s}} |A|^2 \leq C_2 s^{-2} \text{Area}(\mathcal{B}_s). \quad (\text{II.1.23})$$

*Proof.* (Sketch) Since the argument is similar, we sketch only the proof of (II.1.22). By (II.1.2), it is easy to see that

$$\int_{\mathcal{B}_{3s}} |A|^2 \leq 8 s^{-2} \text{Area}(\mathcal{B}_{4s}). \quad (\text{II.1.24})$$

Therefore, to prove (II.1.22), it suffices to find  $s \geq R_0$  with

$$\text{Area}(\mathcal{B}_{4s}) \leq C_2/8 \text{Area}(\mathcal{B}_s). \quad (\text{II.1.25})$$

To do this, we use the bounds for the area given by Proposition II.1.16 to get

$$\left( \min_{1 \leq n \leq m-1} \frac{\text{Area}(\mathcal{B}_{4^n R_0})}{\text{Area}(\mathcal{B}_{4^{n-1} R_0})} \right)^m \leq \frac{\text{Area}(\mathcal{B}_{4^m R_0})}{\text{Area}(\mathcal{B}_{R_0})} \leq C 4^{5m} R_0^3. \quad (\text{II.1.26})$$

Choosing  $m$  large so that  $C R_0^3 \leq 2^m$  and taking the  $m$ -th root of (II.1.26) gives

$$\min_{1 \leq n \leq m-1} \frac{\text{Area}(\mathcal{B}_{4^n R_0})}{\text{Area}(\mathcal{B}_{4^{n-1} R_0})} \leq 2(4^5). \quad (\text{II.1.27})$$

Let  $j$  be where the minimum in (II.1.27) is achieved, so that we get (II.1.25) with  $C_2 = 16(4^5)$  and  $s = 4^{j-1} R_0$ .  $\square$

We will not go into why we need both (II.1.22) and (II.1.23) since this is somewhat technical. One consequence of this doubling property given by (II.1.22) is an average curvature bound for the intrinsic ball  $\mathcal{B}_{3s}$ . Together with the curvature estimate in Proposition II.1.5, this implies that at least “most of”  $\mathcal{B}_{3s}$  has a point-wise scale-invariant curvature bound of the form  $|A|^2 \leq C r^{-2}$ . We will see later that much more is true; namely, most of  $\mathcal{B}_{3s}$  will be almost stable (and therefore satisfy even better estimates). To make this precise, we next discuss a useful way to subdivide intrinsic balls into intrinsic sectors.

Area and total curvature of 1/2-stable sectors. We next define intrinsic sectors and give estimates for the area and total curvature of a 1/2-stable intrinsic sector. Given a curve  $\gamma \subset \partial\mathcal{B}_s$ , define the intrinsic (truncated) sector, see fig. 27,

$$S = S_R(\gamma) = \{\exp_0(v) \mid s \leq |v| \leq s + R \text{ and } \exp_0(sv/|v|) \in \gamma\}. \quad (\text{II.1.28})$$

(Here  $\exp_0 : \mathbf{R}^2 \rightarrow \Sigma$  is the exponential map at 0.) The simplest example of a sector is when  $\Sigma = \mathbf{R}^2$  and  $\gamma$  is given in polar coordinates as  $\{\rho = s, \theta_1 \leq \theta \leq \theta_2\}$ ; in this case, the sector  $S_R(\gamma)$  is just  $\{s \leq \rho \leq s + R, \theta_1 \leq \theta \leq \theta_2\}$ . We will often refer to  $\gamma$  as the inner boundary of the sector and the geodesic rays through  $\partial\gamma$  as the sides of the sector.

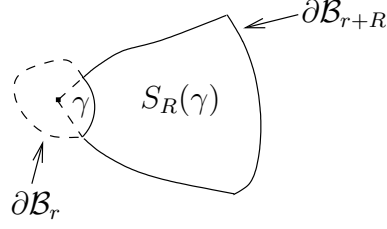


FIGURE 27. An intrinsic sector over a curve  $\gamma$ .

Just as stability led to area bounds for intrinsic balls in (II.1.3), we can bound the area of a  $1/2$ -stable sector. However, to make the cutoff function compactly supported on a sector, we must also cutoff along the inner boundary and along the sides. This introduces new terms in the upper bound for the area. The next lemma, which is an easy consequence of lemma II.1.1 and remark II.1.32 in [CM3], gives the resulting estimate ( $k_g$  is the geodesic curvature of the curve  $\gamma$ ).

**Lemma II.1.29.** [CM3]. Suppose that  $S$  is  $1/2$ -stable,  $\int_\gamma (1 + |k_g| s) \leq C_0 m s$ ,  $R > 2s$ , and for  $x \in S$  we have  $\sup_{\mathcal{B}_{s/4}(x)} |A|^2 \leq C_0 s^{-2}$ . Then for  $\Omega > 2$  and  $2s \leq t \leq 3R/4$

$$t \int_\gamma k_g \leq \text{Length}(\partial \mathcal{B}_t \cap S) \leq C_3 (m + R/s) t, \quad (\text{II.1.30})$$

$$\int_{S_{R/\Omega} \setminus \mathcal{B}_{\Omega s}} |A|^2 \leq C_1 R/s + C_2 m / \log \Omega. \quad (\text{II.1.31})$$

*Proof.* (Sketch). First, as in (II.1.3), we combine the  $1/2$ -stability inequality and the analog of (II.1.2) for intrinsic sectors to get (II.1.30). The  $R/s$  term in (II.1.30) comes from cutting off linearly on a (roughly)  $s$ -tubular neighborhood of the sides of the sector (which have length  $R$ ). Once we have the quadratic area growth given by (II.1.30), we can then use a radial logarithmic cutoff in the stability inequality to get (II.1.31).  $\square$

When we apply Lemma II.1.29, the bound  $\sup_{\mathcal{B}_{s/4}(x)} |A|^2 \leq C_0 s^{-2}$  on  $S$  will be given by starting with a slightly larger  $1/2$ -stable sector and then coming in from the boundary (using a comparison theorem to guarantee that the required intrinsic balls are contained in the larger sector).

Roughly speaking, Lemma II.1.29 shows that if we can find a large  $1/2$ -stable sector, then we can find subsectors with small average curvature. We next explain how this leads to finding a subsector with small total curvature.

Small total curvature of stable subsectors. Given a  $1/2$ -stable sector  $S$  as in Lemma II.1.29 over a long curve  $\gamma$ , we can subdivide  $\gamma$  into subcurves so that one of the sectors over these subcurves has small total curvature. To see this, suppose that  $\text{Length}(\gamma) \approx m s$  for some  $m$  large. If  $m / \log \Omega$  is larger than  $R/s$ , then (II.1.31) says that the truncated sector has small average curvature

$$\int_{S_{R/\Omega} \setminus \mathcal{B}_{\Omega s}} |A|^2 \leq C m / \log \Omega. \quad (\text{II.1.32})$$

If we now subdivide  $\gamma$  into  $m$  subcurves, it follows from (II.1.32) that the truncated sector  $\hat{S}$  over one of these subcurves has small total curvature

$$\int_{\hat{S}} |A|^2 \leq C / \log \Omega. \quad (\text{II.1.33})$$

The  $N$ -valued graph. The next step is to use the  $1/2$ -stable sectors with small total curvature to construct the  $N$ -valued graph  $\Sigma_g$ . To see this, suppose that  $S$  is as in Lemma II.1.29 and  $\hat{S} \subset S$  is a subsector with small total curvature

$$\int_{\hat{S}} |A|^2 \leq \epsilon, \quad (\text{II.1.34})$$

where  $\epsilon > 0$  can be chosen small by taking  $\Omega$  and  $m$  large. The small total curvature (and stability) implies that

$$|A|^2 \leq C \epsilon r^{-2} \text{ on } \hat{S}. \quad (\text{II.1.35})$$

We will use this estimate (II.1.35) to build out  $\Sigma_g$ . For each point  $x$  on the inner boundary of  $\hat{S}$ , let  $\gamma_x \subset \Sigma$  be the geodesic leaving  $x$  orthogonally to  $\partial \hat{S}$ . Integrating the curvature bound (II.1.35) along  $\gamma_x$  implies first that, as a curve in  $\mathbf{R}^3$ ,  $\gamma_x$  has small total geodesic curvature and is close to a line segment. Second, it also implies that the unit normal  $\mathbf{n}$  to  $\Sigma$  has small oscillation along  $\gamma_x$ . It is now easy to see that as we vary the initial point  $x$  on the inner boundary of  $\hat{S}$ , the geodesics  $\gamma_x$  trace out a multi-valued graph  $\Sigma_g$ .

Finally, we review how these steps fit together to prove Theorem II.0.14.

**Sketch of the proof of Theorem II.0.14:** After rescaling by  $C/r_0$ , we can assume that

$$\sup_{B_C \cap \Sigma} |A|^2 \leq 4 |A|^2(0) = 4. \quad (\text{II.1.36})$$

The key for proving Theorem II.0.14 is to find many large intrinsic sectors with a quadratic curvature bound. To do this, we first fix some large  $\bar{m}$  and use Proposition II.1.5 and the lower bound  $|A|^2(0) = 1$  in (II.1.36) to get  $R_0$  so that for  $R \geq R_0$

$$\text{Length}(\partial \mathcal{B}_R) \geq \bar{m} R. \quad (\text{II.1.37})$$

Using the upper bound  $|A|^2 \leq 4$  in (II.1.36), we can apply Corollary II.1.21 to get  $R_3 > R_0$  and many long disjoint curves  $\tilde{\gamma}_i \subset \partial \mathcal{B}_{R_3}$  so the sectors over  $\tilde{\gamma}_i$  have uniformly bounded total curvature  $\int |A|^2$ . Proposition II.1.5 then gives a (point-wise) quadratic curvature bound on these sectors.

Now that we have these many disjoint sectors with a quadratic curvature bound (as many as we want by taking  $\bar{m}$  large), two must be close together and, hence, also  $1/2$ -stable. Lemma II.1.29 gives a subsector with small total curvature which then must contain the  $N$ -valued graph  $\Sigma_g$  (this is done in corollary II.1.34 of [CM3]).

## II.2. THE ESTIMATE BETWEEN THE SHEETS AND THE EXTENSION OF MULTI-VALUED GRAPHS

In this section, we will give an overview of the proof of Theorem II.0.16 where we extend the multi-valued graphs almost to the boundary corresponding to B. in fig. 23. This result is significantly more subtle than the local existence result discussed in the previous section. We only give a very rough outline of the proof and refer to [CM3] for the full story.

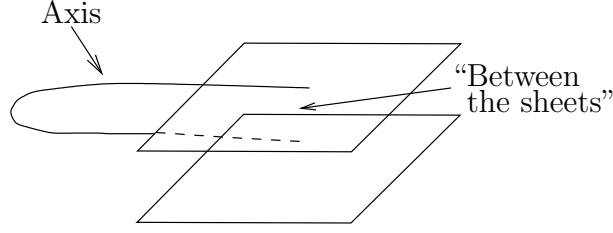


FIGURE 28. The estimate between the sheets; Theorem II.2.1.

The key component of the proof of the extension theorem is a curvature estimate “between the sheets” for embedded minimal disks in  $\mathbf{R}^3$ . We will think of an axis (see fig. 29) for such a disk  $\Sigma$  as a point or curve away from which the surface locally (in an extrinsic ball) has more than one component. With this weak notion of an axis, our estimate is that if one component of  $\Sigma$  is sandwiched between two others that connect to an axis, then the one that is sandwiched has curvature estimates; see Theorem II.2.1. The example to keep in mind is a helicoid and the components are “consecutive sheets” away from the axis.

Let  $\gamma_{p,q}$  denote the line segment from  $p$  to  $q$  and  $T_s(\gamma_{p,q})$  its  $s$ -tubular neighborhood. A curve  $\gamma$  is  $h$ -almost monotone if given  $y \in \gamma$ , then  $B_{4h}(y) \cap \gamma$  has only one component which intersects  $B_{2h}(y)$ . Our curvature estimate “between the sheets” is:

**Theorem II.2.1.** (Theorem I.0.8 in [CM3]). See fig. 29. There exist  $c_1 \geq 4$ ,  $2c_2 < c_4 < c_3 \leq 1$  so: Let  $\Sigma \subset B_{c_1 r_0}$  be an embedded minimal disk with  $\partial\Sigma \subset \partial B_{c_1 r_0}$  and  $y \in \partial B_{2r_0}$ . Suppose  $\Sigma_1, \Sigma_2, \Sigma_3$  are distinct components of  $B_{r_0}(y) \cap \Sigma$  and  $\gamma \subset (B_{r_0} \cup T_{c_2 r_0}(\gamma_{0,y})) \cap \Sigma$  is a curve with  $\partial\gamma = \{y_1, y_2\}$  where  $y_i \in B_{c_2 r_0}(y) \cap \Sigma_i$  and each component of  $\gamma \setminus B_{r_0}$  is  $c_2 r_0$ -almost monotone. Then any component  $\Sigma'_3$  of  $B_{c_3 r_0}(y) \cap \Sigma_3$  with  $y_1, y_2$  in distinct components of  $B_{c_4 r_0}(y) \setminus \Sigma'_3$  is a graph.

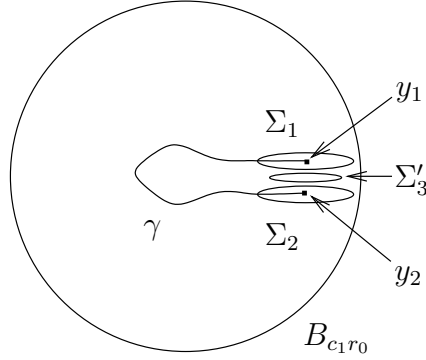


FIGURE 29.  $y_1, y_2, \Sigma_1, \Sigma_2, \Sigma'_3$ , and  $\gamma$  in Theorem II.2.1.

The idea of the proof of Theorem II.2.1 is to show that if this were not the case, then we could find an embedded stable disk that would be almost flat and lie in the complement of the original disk. In fact, we can choose the stable disk to be sandwiched between the two components as well. The flatness would force the stable disk to eventually cross the axis in the original disk, contradicting that they were disjoint.

The curve  $\gamma$  in Theorem II.2.1 which plays the role of an axis and connects  $\Sigma_1$  and  $\Sigma_2$  can in many instances be extended using the maximum principle once it occurs on a given small scale; cf. lemma I.0.11 of [CM3]. This is used both in the proof of Theorem II.2.1 and in the applications of it.

**Overview of the proof of Theorem II.0.16:** The first step (part I of [CM3]) is to show Theorem II.2.1 when the surface is in a slab; i.e., when  $\Sigma \subset \{|x_3| \leq \beta h\}$ .

The second step (part II of [CM3]) is to show that certain stable disks starting off as multi-valued graphs remain multi-valued graphs as the outer radius increases. This is needed when we generalize the results of step one to when the surface is not anymore in a slab.

Two facts go into the proof of the extension of stable disks. First, we show that if an almost flat multi-valued graph sits inside a stable disk, then the outwardly defined intrinsic sector from a curve which is a multi-valued graph over a circle has a subsector which is almost flat; cf. Lemma II.1.29 and the paragraph “Small total curvature of stable subsectors” above. As the initial multi-valued graph becomes flatter and the number of sheets in it goes up, the subsector becomes flatter. The second fact is that the separation between the sheets grows sublinearly; (I.1.2).

The first application of these two facts is to extend the middle sheet as a multi-valued graph. This is done by dividing the initial multi-valued graph (or curve in the graph that is itself a multi-valued graph over the circle) into three parts where the middle sheet is the second part. The idea is then that the first and third parts have subsectors which are almost flat multi-valued graphs and the middle part (which has curvature estimates since it is stable) is sandwiched between the two others. Hence its sector is also almost flat.

A thing that adds some technical complications to the above picture is that in the result about almost flat subsectors it is important that the ratio between the size of the initial multi-valued graph and how far one can go out is fixed. This is because the estimate for the subsector comes from a total curvature estimate which is in terms of this ratio (see (II.1.31)) and can only be made small by looking at a fixed large number of rotations for the graph. This forces us to successively extend the multi-valued graph. The issue is then to make sure that as we move out in the sector and repeat the argument we have essentially not lost sheets. This is taken care of by using the sublinear growth of the separation between the sheets together with the Harnack inequality and the maximum principle. (The maximum principle is used to make sure that as we try to recover sheets after we have moved out then we don't hit the boundary of the disk before we have recovered essentially all of the sheets that we started with.) The last thing which is used is theorem 3.36 in [CM10]. This is used to guarantee that, as we patch together these multi-valued graphs coming from different scales, then the surface that we get is still a multi-valued graph over a fixed plane.

The third step (part III of [CM3]) is to generalize the curvature estimate between the sheets to the case where the surface is not anymore in a slab. This uses the extension of the stable graphs from step two.

Finally, using steps one, two, and three we showed Theorem II.0.16 in part IV of [CM3].

### Part III. The proof of the one-sided curvature estimate

In appendix A of [CM6] we showed curvature estimates for minimal hyper-surfaces in  $\mathbf{R}^n$  which on all sufficiently small scales lie on one side of, but come close to, a hyper-plane.

Such a scale invariant version of Theorem I.3.3 can (unlike Theorem I.3.3) be proven quite easily by a blow up argument using the minimal surface equation. Moreover, such a scale invariant condition is very similar to the classical Reifenberg property. (After all, a subset of  $\mathbf{R}^n$  has the Reifenberg property if it is close on all scales to a hyper-plane.) As explained in Part I (in particular Corollary I.3.8), the significance of Theorem I.3.3 is indeed that it only requires closeness on one scale. On the other hand, this is what makes it difficult to prove and requires us to use the results discussed in the previous parts together with results from [CM5].

Let us briefly outline the proof of the one-sided; i.e., Theorem I.3.3. Suppose that  $\Sigma$  is an embedded minimal disk in the half-space  $\{x_3 > 0\}$ . We prove the curvature estimate by contradiction; so suppose that  $\Sigma$  has low points with large curvature. Starting at such a point, we decompose  $\Sigma$  into disjoint multi-valued graphs using the existence of nearby points with large curvature given by corollary III.3.5 of [CM5], a blow up argument, and [CM3], [CM4]. The key point is then to show (see Proposition III.0.2 below) that we can in fact find such a decomposition where the “next” multi-valued graph starts off a definite amount below where the previous multi-valued graph started off. In fact, what we show is that this definite amount is a fixed fraction of the distance between where the two graphs started off. Iterating this eventually forces  $\Sigma$  to have points where  $x_3 < 0$ . This is the desired contradiction.

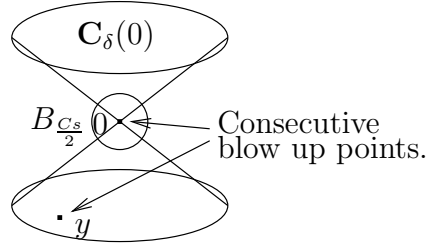


FIGURE 30. Proposition III.0.2: Two consecutive blow up points satisfying (III.0.4).

**Proposition III.0.2.** (See proposition III.2.2 in [CM6] for the precise statement). See fig. 30. There exists  $\delta > 0$  such that if  $(0, s)$  satisfies (III.0.4) and  $\Sigma_0 \subset \Sigma$  is the corresponding (to  $(0, s)$ ) 2-valued graph over  $D_R \setminus D_s$ , then we get  $(y, t)$  satisfying (III.0.4) with  $y \in C_\delta(0) \cap \Sigma \setminus B_{C_s/2}$  and where  $y$  is below  $\Sigma_0$ .

To prove this key proposition (Proposition III.0.2), we use two decompositions and two kinds of blow up points. The first decomposition uses the more standard blow up points given as pairs  $(y, s)$  where  $y \in \Sigma$  and  $s > 0$  is such that

$$\sup_{B_{8s}(y)} |A|^2 \leq 4|A|^2(y) = 4C_1^2 s^{-2}. \quad (\text{III.0.3})$$

The point about such a pair  $(y, s)$  is that by [CM3], [CM4] (and an argument in section II.2 of [CM6] which allows us replace extrinsic balls by intrinsic ones), then  $\Sigma$  contains a multi-valued graph near  $y$  starting off on the scale  $s$ . (This is assuming that  $C_1$  is a sufficiently large constant given by [CM3], [CM4].) The second kind of blow up points are the ones

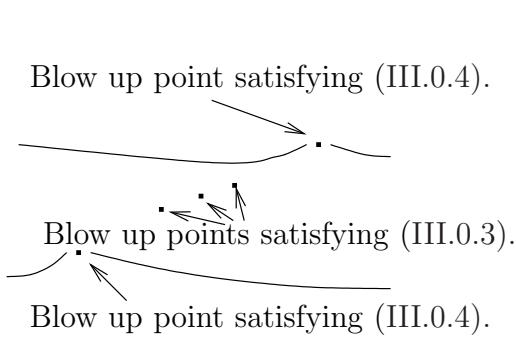


FIGURE 31. Between two consecutive blow up points satisfying (III.0.4) there are a bunch of blow up points satisfying (III.0.3).

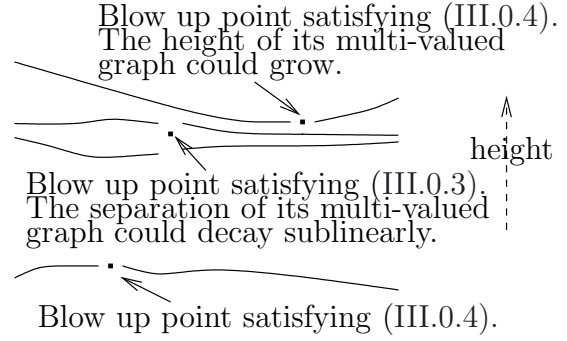


FIGURE 32. Measuring height. Blow up points and corresponding multi-valued graphs.

where (except for a technical issue) 8 is replaced by some really large constant  $C$ , i.e.,

$$\sup_{\mathcal{B}_{Cs}(y)} |A|^2 \leq 4|A|^2(y) = 4C_1^2 s^{-2}. \quad (\text{III.0.4})$$

The point will then be that we can find blow up points satisfying (III.0.4) so that the distance between them is proportional to the sum of the scales. Moreover, between consecutive blow up points satisfying (III.0.4), we can find a bunch of blow up points satisfying (III.0.3); see fig. 31. The advantage is now that if we look between blow up points satisfying (III.0.4), then the height of the multi-valued graph given by such a pair grows like a small power of the distance whereas the separation between the sheets in a multi-valued graph given by (III.0.3) decays like a small power of the distance; see fig. 32. Now thanks to that the number of blow up points satisfying (III.0.3) (between two consecutive blow up points satisfying (III.0.4)) grows almost linearly then, even though the height of the graph coming from the blow up point satisfying (III.0.4) could move up (and thus work against us), then the sum of the separations of the graphs coming from the points satisfying (III.0.3) dominates the other term. Thus the next blow up point satisfying (III.0.4) (which lies below all the other graphs) is forced to be a definite amount lower than the previous blow up point satisfying (III.0.4).

#### Part IV. The local case - when singular limit laminations can occur

In this part we discuss the differences between the so-called local and global cases. The local case is where we have a sequence of embedded minimal disks in a ball of fixed radius in  $\mathbf{R}^3$  - the global case is where the disks are in a sequence of expanding balls with radii tending to infinity. The main difference between these cases is that in the local case we can get limits with singularities. In the global case this does not happen because in fact any limit is a foliation by flat parallel planes (assuming that the curvatures of the sequence are blowing up).

To precisely define the local and global cases, suppose  $\Sigma_i \subset B_{R_i} = B_{R_i}(0) \subset \mathbf{R}^3$  with  $\partial\Sigma_i \subset \partial B_{R_i}$  is a sequence of (compact) embedded minimal disks and either:

- (a)  $R_i$  equal to a finite constant.
- (b)  $R_i \rightarrow \infty$ .



Case (a) is what we call the *local case* and (b) is what we refer to as the *global case*; Theorem I.0.5 dealt with the global case. Recall that a surface  $\Sigma \subset \mathbf{R}^3$  is said to be properly embedded if it is embedded and the intersection of  $\Sigma$  with any compact subset of  $\mathbf{R}^3$  is compact. We say that a lamination or foliation is proper if each leaf is proper.

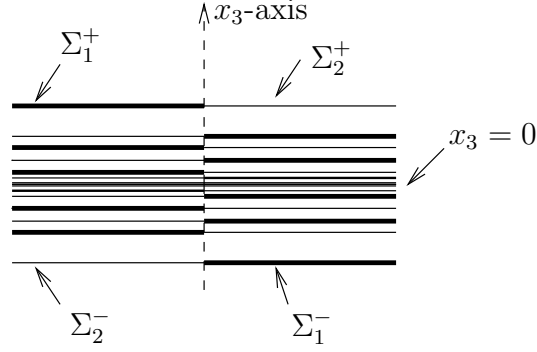


FIGURE 33. A schematic picture of the limit in Theorem IV.0.6 which is not smooth and not proper (the dotted  $x_3$ -axis is part of the limit). The limit contains four multi-valued graphs joined at the  $x_3$ -axis;  $\Sigma_1^+$ ,  $\Sigma_2^+$  above the plane  $x_3 = 0$  and  $\Sigma_1^-$ ,  $\Sigma_2^-$  below the plane. Each of the four spirals into the plane.

To explain the difference between the two cases, we consider sequences of minimal disks  $\Sigma_i$  as above where the curvatures blow up, e.g.,

$$\lim_{i \rightarrow \infty} \sup_{B_1 \cap \Sigma_i} |A|^2 = \infty. \quad (\text{IV.0.5})$$

(Of course, if the curvatures do not blow up, then the Arzela-Ascoli theorem easily gives smooth convergence of a subsequence in either case.) In the global case, Theorem I.0.5 gives a subsequence of the  $\Sigma_i$  converging off of a Lipschitz curve to a foliation by parallel planes. In particular, the limit is a (smooth) foliation which is proper. However, we showed in [CM16] (see Theorem IV.0.6 below) that smoothness and properness of the limit can fail in the local case; cf. fig. 33.

To illustrate the key issue for the failure of properness, suppose that  $|A|^2(0) \rightarrow \infty$  as  $i \rightarrow \infty$ . In either the local or global case (see Section I.3), we get a sequence of 2-valued graphs which converges to a minimal graph  $\Sigma_0$  through 0 (this graph is a plane in the global case). Furthermore, by the one-sided curvature estimate (see Corollary I.3.8), the intersection of  $\Sigma_i$  with a low cone about  $\Sigma_0$  consists of multi-valued graphs for  $i$  large. There are now two possibilities:

- The multi-valued graphs in this low cone close up in the limit.
- The limits of these multi-valued graphs spiral infinitely into  $\Sigma_0$ .

In the first case, where properness holds, the sequence converges to a foliation in a neighborhood of 0. In the second case, where properness fails, the sequence converges to a lamination away from 0 but cannot be extended smoothly to any neighborhood of 0. The proof of properness in the global case is described in Section I.2.

In the local case, Theorem IV.0.6 constructs a sequence of disks  $\Sigma_i \subset B_1$  as above where the curvatures blow up only at 0 and  $\Sigma_i \setminus \{x_3\text{-axis}\}$  consists of two multi-valued graphs for each  $i$ ; see (1), (2), and (3). Furthermore (see (4)),  $\Sigma_i \setminus \{x_3 = 0\}$  converges to two embedded minimal disks  $\Sigma^- \subset \{x_3 < 0\}$  and  $\Sigma^+ \subset \{x_3 > 0\}$  each of which spirals into  $\{x_3 = 0\}$  and thus is not proper; see fig. 33.

**Theorem IV.0.6.** (Theorem 1 in [CM16]). See fig. 33. There is a sequence of compact embedded minimal disks  $0 \in \Sigma_i \subset B_1 \subset \mathbf{R}^3$  with  $\partial\Sigma_i \subset \partial B_1$  and containing the vertical segment  $\{(0, 0, t) \mid |t| < 1\} \subset \Sigma_i$  so:

- (1)  $\lim_{i \rightarrow \infty} |A_{\Sigma_i}|^2(0) = \infty$ .
- (2)  $\sup_i \sup_{\Sigma_i \setminus B_\delta} |A_{\Sigma_i}|^2 < \infty$  for all  $\delta > 0$ .
- (3)  $\Sigma_i \setminus \{x_3\text{-axis}\} = \Sigma_{1,i} \cup \Sigma_{2,i}$  for multi-valued graphs  $\Sigma_{1,i}$  and  $\Sigma_{2,i}$
- (4)  $\Sigma_i \setminus \{x_3 = 0\}$  converges to two embedded minimal disks  $\Sigma^\pm \subset \{\pm x_3 > 0\}$  with  $\overline{\Sigma^\pm} \setminus \Sigma^\pm = B_1 \cap \{x_3 = 0\}$ . Moreover,  $\Sigma^\pm \setminus \{x_3\text{-axis}\} = \Sigma_1^\pm \cup \Sigma_2^\pm$  for multi-valued graphs  $\Sigma_1^\pm$  and  $\Sigma_2^\pm$  which spiral into  $\{x_3 = 0\}$ ; see fig. 33.

It follows from (4) that  $\Sigma_i \setminus \{0\}$  converges to a lamination of  $B_1 \setminus \{0\}$  (with leaves  $\Sigma^-$ ,  $\Sigma^+$ , and  $B_1 \cap \{x_3 = 0\} \setminus \{0\}$ ) which does not extend to a lamination of  $B_1$ . Namely, 0 is not a removable singularity.

The example in Theorem IV.0.6 was constructed using the Weierstrass representation. Recall that if  $\Omega \subset \mathbf{C}$  is a domain, then the classical Weierstrass representation starts from a meromorphic function  $g$  on  $\Omega$  and a holomorphic one-form  $\phi$  on  $\Omega$  and associates a (branched) conformal minimal immersion  $F : \Omega \rightarrow \mathbf{R}^3$  by

$$F(z) = \operatorname{Re} \int_{\zeta \in \gamma_{z_0, z}} \left( \frac{1}{2} (g^{-1}(\zeta) - g(\zeta)), \frac{i}{2} (g^{-1}(\zeta) + g(\zeta)), 1 \right) \phi(\zeta). \quad (\text{IV.0.7})$$

Here  $z_0 \in \Omega$  is a fixed base point and the integration is along a path  $\gamma_{z_0, z}$  from  $z_0$  to  $z$ . The choice of  $z_0$  changes  $F$  by adding a constant. When  $g$  has no zeros or poles and  $\Omega$  is simply connected, then  $F(z)$  does not depend on the choice of path  $\gamma_{z_0, z}$ .

**Sketch of the proof of Theorem IV.0.6:** We construct a one-parameter family (with parameter  $a \in (0, 1/2)$ ) of minimal immersions  $F_a$  by making a specific choice of Weierstrass data  $g = e^{ih_a}$  (where  $h_a = u_a + i v_a$ ),  $\phi = dz$ , and domain  $\Omega_a$  to use in (IV.0.7). Namely, for each  $0 < a < 1/2$ , we define

$$h_a(z) = \frac{1}{a} \arctan\left(\frac{z}{a}\right) \text{ on } \Omega_a = \{(x, y) \mid |x| \leq 1/2, |y| \leq (x^2 + a^2)^{3/4}/2\}. \quad (\text{IV.0.8})$$

Note that the function  $h_a$  is well-defined since  $\Omega_a$  is simply connected and  $\pm i a \notin \Omega_a$ .

It remains to verify that this sequence of minimal immersions has the desired properties. Properties (1) and (2) in Theorem IV.0.6 follow easily from calculating the curvature  $K_a$

$$K_a(z) = \frac{-|\partial_z h_a|^2}{\cosh^4 v_a} = \frac{-|z^2 + a^2|^{-2}}{\cosh^4(\operatorname{Im} \arctan(z/a)/a)}. \quad (\text{IV.0.9})$$

Properties (3) and (4) as well as the convergence away from 0 follow rather easily by integrating the equations (IV.0.7). The key point in the proof, and only remaining point, is to show that the immersions  $F_a : \Omega_a \rightarrow \mathbf{R}^3$  are embeddings. We do this by showing that each vertical line segment in the domain  $\Omega_a$  is mapped by  $F_a$  to curve in a horizontal plane (i.e.,

a plane where  $x_3$  is constant) and each such curve is a graph over a fixed line segment; see [CM16] for the details.

## REFERENCES

- [ChC] J. Cheeger and T. H. Colding, On the Structure of Spaces with Ricci Curvature Bounded Below; I, *Jour. of Diff. Geometry* 46 (1997) 406-480.
- [CM1] T.H. Colding and W.P. Minicozzi II, Minimal surfaces, Courant Lecture Notes in Math., v. 4, 1999.
- [CM2] T.H. Colding and W.P. Minicozzi II, Estimates for parametric elliptic integrands, *International Mathematics Research Notices*, no. 6 (2002) 291-297.
- [CM3] T.H. Colding and W.P. Minicozzi II, The space of embedded minimal surfaces of fixed genus in a 3-manifold I; Estimates off the axis for disks, math.AP/0210106.
- [CM4] T.H. Colding and W.P. Minicozzi II, The space of embedded minimal surfaces of fixed genus in a 3-manifold II; Multi-valued graphs in disks, math.AP/0210086.
- [CM5] T.H. Colding and W.P. Minicozzi II, The space of embedded minimal surfaces of fixed genus in a 3-manifold III; Planar domains, math.AP/0210141.
- [CM6] T.H. Colding and W.P. Minicozzi II, The space of embedded minimal surfaces of fixed genus in a 3-manifold IV; Locally simply connected, math.AP/0210119.
- [CM7] T.H. Colding and W.P. Minicozzi II, The space of embedded minimal surfaces of fixed genus in a 3-manifold V; Fixed genus, in preparation.
- [CM8] T.H. Colding and W.P. Minicozzi II, Multi-valued minimal graphs and properness of disks, *International Mathematics Research Notices*, no. 21 (2002) 1111-1127.
- [CM9] T.H. Colding and W.P. Minicozzi II, On the structure of embedded minimal annuli, *International Mathematics Research Notices*, no. 29 (2002) 1539-1552.
- [CM10] T.H. Colding and W.P. Minicozzi II, Minimal annuli with and without slits, *Jour. of Symplectic Geometry*, vol. 1, issue 1 (2001) 47-61.
- [CM11] T.H. Colding and W.P. Minicozzi II, Complete properly embedded minimal surfaces in  $\mathbf{R}^3$ , *Duke Math. J.* 107 (2001), no. 2, 421-426.
- [CM12] T.H. Colding and W.P. Minicozzi II, Convergence of embedded minimal surfaces without area bounds in three manifolds, *C.R. Acad. Sci. Paris t. 327, Série I* (1998) 765-770.
- [CM13] T.H. Colding and W.P. Minicozzi II, Removable singularities for minimal limit laminations, *C.R. Acad. Sci. Paris t. 331, Série I* (2000) 465-468.
- [CM14] T.H. Colding and W.P. Minicozzi II, Embedded minimal surfaces without area bounds in 3-manifolds. Geometry and topology: Aarhus (1998), 107-120, *Contemp. Math.*, 258, Amer. Math. Soc., Providence, RI, 2000.
- [CM15] T.H. Colding and W.P. Minicozzi II, Disks that are double spiral staircases, *Notices of the AMS*, Vol. 50, no. 3, (2003) 327-339.
- [CM16] T.H. Colding and W.P. Minicozzi II, Embedded minimal disks: Proper versus nonproper - global versus local, *Transactions of the AMS*, to appear. math.DG/0210328.
- [CM17] T.H. Colding and W.P. Minicozzi II, An excursion into geometric analysis, *Surveys in Differential Geometry*, IX.
- [MeRo] W. Meeks III and H. Rosenberg, The uniqueness of the helicoid and the asymptotic geometry of properly embedded minimal surfaces with finite topology, preprint.

COURANT INSTITUTE OF MATHEMATICAL SCIENCES AND PRINCETON UNIVERSITY, 251 MERCER STREET, NEW YORK, NY 10012 AND FINE HALL, WASHINGTON RD., PRINCETON, NJ 08544-1000

DEPARTMENT OF MATHEMATICS, JOHNS HOPKINS UNIVERSITY, 3400 N. CHARLES ST., BALTIMORE, MD 21218

*E-mail address:* colding@cims.nyu.edu, minicozz@jhu.edu